Aerospace Science and Technology 161 (2025) 110145

Contents lists available at ScienceDirect

Aerospace Science and Technology

journal homepage: www.elsevier.com/locate/aescte

Control allocation problem transformation approaches for over-actuated vectored thrust VTOLs

Emmanuel Enenakpogbe [*], James F. Whidborne, Linghai Lu

Dynamics, Simulation & Control Group, Centre for Aeronautics, School of Aerospace, Transport and Manufacturing, Cranfield University, Bedfordshire, United Kingdom

ARTICLE INFO

Communicated by Jayaram Sanjay

Keywords:
Effector mapping
Active Set
Optimal
Real-time
Linear Time Varying (LTV)
Constrained
Incremental

ABSTRACT

One main challenge of vectored thrust VTOLs is actuator thrust control saturation because it may lead to undesired behaviour and loss of control if the control channels are not prioritised. Another challenge of vectored thrust VTOLs is that the vectored thrust results in non-linear effector mapping preventing the direct use of standard linear control allocation approaches. Linear control allocation approaches have lower online computational and complexity burden, and have simplier requirements for fault tolerance and reconfigurability than nonlinear control allocation approaches. This paper proposes three real-time control allocation approaches for transforming a nonlinear control allocation problem to a linear problem so that classical linear control allocation approaches can then be used. The approaches which addresses the two main challenges of the particular VTOL configuration are then tested using three selected flight test manoeuvres on a generic over-actuated vectored thrust three degrees of freedom planar VTOL with no aerodynamics. The first approach transfers the non-linearity from the effector mapping to the computation of the actuator limits by formulating the real controls in cartesian form and then converts the physical actuator limits from polar to cartesian form. The second approach transforms the non-linear effector mapping to a linear mapping via numerical linearisation of the non-linear effector mapping in real-time. The third approach is similar to second approach except an extra step which transforms the virtual controls from cartesian to polar before performing an analytical linearisation resulting in a different and more complicated linear Effector mapping.

The results demonstrate the effectiveness of the proposed control allocation schemes to allocate remaining control authority to higher priority and critical control channels in order to maintain operational safety and stability during certain flight conditions while there is limited control authority.

1. Introduction

Vectored thrust eVTOLs, one common category of eVTOLs according to the Vertical Flight Society (VFS) [37,38], are supported in vertical takeoff and landing flight by the horizontally-mounted propulsion systems, directing thrust downwards to generate lift. Horizontal flight is supported primarily by lift generated from the wings, with some or all of the propulsion systems rotated to the required position to provide horizontal thrust for forward speed. An example of an over-actuated vectored thrust VTOL is the Lilium Jet [18].

One main challenge of VTOLs is that they are overactuated (equipped with more effectors than the degrees of freedom they control), thus introducing redundancy in case of effector failure [20,29,34] in order to ensure the required levels of reliability and safety in the emerging UAM industry. This over-actuation creates the challenge of allocating the overall control demand to individual redundant effectors during both normal and degraded operation known as control allocation (CA). CA provides an optimised allocation of control effectors for the various degrees of freedom under fault-free operation, optimization of actuator utilization (including secondary objectives like drag, wing load reduction etc.) with respect to varying flight phases and provide scope for reconfiguration in the event of a fault in the control effector.

A second challenge of this configuration is that the vectored thrust results in non-linear effector mapping (control effectiveness mapping) preventing the direct use of classical linear control allocation approaches and consequent computational infeasibility of performing non-linear

* Corresponding author.
E-mail addresses: E.Enenakpogbe@cranfield.ac.uk (E. Enenakpogbe), j.f.whidborne@cranfield.ac.uk (J.F. Whidborne), l.lu@cranfield.ac.uk (L. Lu).
URLs: https://orcid.org/0000-0001-7610-682X (E. Enenakpogbe), https://orcid.org/0000-0002-6310-8946 (J.F. Whidborne), https://orcid.org/0000-0002-2688-7944 (L. Lu).

https://doi.org/10.1016/j.ast.2025.110145
Received 6 September 2024; Received in revised form 14 January 2025; Accepted 13 March 2025
Available online 18 March 2025
1270-9638/© 2025 The Author(s). Published by Elsevier Masson SAS. This is an open access article under the CC BY license (http://creativecommons.org/licenses/by/4.0/).

Nomenclature

Abbreviations

Abs	absolute
ACM	aircraft control manoeuvre
An	analytical
AS	active Set
CA	control allocation
Cart	cartesian
CTL	control laws
Con	constraints
DoF	degrees of freedom
Eff	effector
eVTOL	Electrical Vertical Take-Off and Landing
FTM	flight test manoeuvre
Incr	Incremental
LTV	Linear Time Varying
Num	numerical
Pol	polar
UAM	Urban Air Mobility
UAV	Unmanned Air Vehicle
VTOL	Vertical Take-Off and Landing
WLS	Weighted Least Squares

Nomenclature

$*_a$	rear/aft rotor
$*_f$	front/fore rotor
$\mathbf{B}_{as}$	Active Set row augumented weighted virtual control matrix
$\bar{*}$	maximum limit
$\mathbf{B}_u$	linear control effectiveness matrix
$\mathbf{C}$	actuator rate constraints $\dot{\mathbf{u}}_{\min}$ and $\dot{\mathbf{u}}_{\max}$
$\mathbf{G}_u$	LTV control effectiveness matrix
$\mathbf{B}_\mathbf{u}^+$	Moore-Penrose inverse of the linear control effectiveness matrix
$\boldsymbol{\tau}$	actual generalised forces and moments
$\boldsymbol{\tau_c}$	virtual or overall aircraft control command
$\mathbf{U}$	actuator saturation constraints $\mathbf{u}_{\min}$ and $\mathbf{u}_{\max}$
Δ	control change or increment from previous to current software iteration
δ	complementary filter gain used for drift correct in incremental CA Approaches
Δt	sampling period or time increment from previous to current software iteration
$\dot{\bar{*}}$	maximum rate limit
$\dot{\underline{*}}$	minimum rate limit
$\mathbf{e}$	NDI high-level CTL inner loop control error vector
$\mathbf{f}$	non-linear system plant state transition matrix
$\mathbf{F}(\mathbf{x})$	product of (Jacobian $\frac{\partial \mathbf{h}}{\partial \mathbf{x}}$ of output matrix h with respect to $\mathbf{x}$) and $f(\mathbf{x})$
$\mathbf{g}$	affine non-linear control effectiveness matrix
$\mathbf{G}(\mathbf{x})$	product of (Jacobian $\frac{\partial \mathbf{h}}{\partial \mathbf{x}}$ of output matrix $\mathbf{h}$ with respect to $\mathbf{x}$) and $\mathbf{u}$
Γ	effector tilt angle
γ	primary objective weighting factor ensuring $W_u \ll W_v$
Γ_0	actuator tilt angle at time $t = 0$ or previous software iteration
$\mathbf{G}_\mathbf{u}^+$	Moore-Penrose inverse of the LTV control effectiveness matrix
$\mathbf{h}$	output matrix
$\mathbf{K}$	NDI outer loop (feedback) linear controller gain vector
$\mathbf{K}_{\text{out}}$	high-level CTL outerloop linear controller
λ	flight path angle
$\mathbf{I}_n$	the $n \times n$ identity matrix
$\mathbf{p}$	Active Set perturbation on the real controls
$\mathbf{q}$	Active Set row augumented weighted real control matrix
$\mathbf{r}$	high-level CTL vector of reference signals to be tracked
$\mathbf{s}$	slack variable representing the control error in all control channels and degrees of freedom
θ	pitch angle
$\mathbf{u}$	vector of effector demands or real controls
$\mathbf{u}_p$	preferred actuator position
$\mathbf{u}_{cp}$	drift-compensated actuator position using complimentary filter
$\mathbf{u}_{op}$	optimal actuator position
$\mathbf{u}_{uc}$	unconstrained actuator position using Moore-Penrose inverse
$\mathbf{u}_{x,z}$	vector of real controls in Cartesian form (the x- and z- coordinate rotor thrust components)
$\underline{*}$	minimum limit
$\mathbf{v}$	NDI high-level CTL outer loop controller output vector
$\mathbf{W}_u$	actuator utilization or prioritization weight positive definite matrix
$\mathbf{W}_v$	weight matrix or control channel priority matrix
$\mathbf{x}$	vector of state variables
$\mathbf{y}$	NDI high-level CTL vector of outputs to be controlled
F_X	overall vehicle (virtual) propulsive thrust in the body x-direction
F_Z	overall vehicle (virtual) propulsive thrust in the body z-direction
g	gravitational acceleration constant
i_{max}	maximum number of Active Set control allocation optimisation software iterations
I_{yy}	moment of inertia about the y-body direction
J	secondary objective cost function
m	vehicle mass
M_a	net aerodynamic moment acting about the body y-direction
M_T	net vehicle pitching moment acting about the body y-direction
q	pitch rate
T	effector thrust
T_0	actuator thrust at time $t = 0$ or previous software iteration
T_{X*}	front and rear/aft rotor thrust in the body x-direction
T_{Z*}	front and rear/aft rotor thrust in the body z-direction
u	horizontal velocity in the body x-axis direction
V	airspeed
w	vertical velocity in the body z-axis direction
X	net aerodynamic force acting at the centre of gravity in the body x axis
x	horizontal position of the centre of gravity of the vehicle
Z	net aerodynamic force acting at the centre of gravity in the body z axis
z	vertical position of the centre of gravity of the vehicle

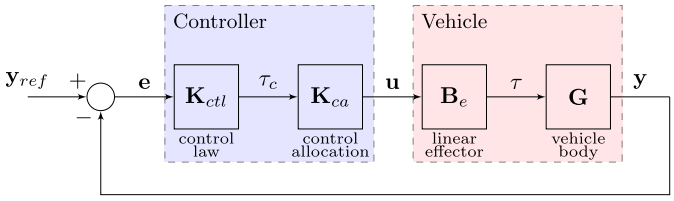

Fig. 1. General Linear Control Allocation Scheme.

programming in real time. The vectored thrust effector mapping non-linearity is due to the fact that the virtual controls (aircraft-level generalised forces and moments) are combination of the thrust and sine and cosine functions of the tilt angle even ignoring any non-linearity in the propulsion (mapping of rpm to thrust) which is outside the scope of this work. This presents a challenge in allocating the overall control demand to the individual actuators for VTOL configurations with vectored thrust effectors even without considering any degree of over-actuation. Nonlinear control allocation approaches would be required to resolve the control allocation of an effector configuration such as vectored thrust effector if either the effector mapping or cost function (e.g. non-quadratic) are not linear, or the constraint sets are not polyhedral. Explicit solutions can be found for linear effector models in combination with simple objective functions and constraints, while iterative numerical procedures are required for the more complicated problems [15]. For nonlinear and possibly non-convex optimization problems where issues such as numerical robustness, convergence to non-global minimums, computational complexity and reliability of the numerical software implementation exist, particular attention will be needed to address such issues.

There are several linear and nonlinear control allocation approaches and techniques proposed for motion control of over-actuated mechanical systems [6,10,15]. Some control allocation techniques for over-actuated UAVs and drones are studied in [3,21,26,30,39,42,44]. Control allocation approaches for linear and nonlinear effector models are reviewed in [15], and include unconstrained linear control allocation approaches, constrained linear control allocation approaches and constrained nonlinear control allocation.

Several unconstrained linear control allocation approaches are reviewed [6], and include generalized inverses or pseudoinverses, Moore-Penrose pseudo-inverse and Singular Value Decomposition based (SVD-based) Generalised inverses whereby no actuator constraints are applied and the effector mapping is linear. Meanwhile, constrained Linear control allocation approaches which applies effector constraints but only for systems with linear effector mapping are reviewed in [15] include redistributed pseudo-inverse, cascaded generalised inverse (CGI), daisy chaining, direct control allocation, simplex numerical linear programming, Active Set (AS) numerical quadratic programming method, Interior Point numerical quadratic programming method, iterative fixed-point numeric quadratic programming method, multi-parametric quadratic programming, binary search trees, lattice representations, decomposition approach for master and slave problems, an optimization-based control allocation method integrated with a parameter estimation scheme, Fault tolerant Optimization-based control allocation, dynamic control allocation approach, Model Predictive Control (MPC) optimisation-based control approach etc.

Control allocation approaches for nonlinear effector models are reviewed in [15] and include nonlinear programming for control allocation, Sequential Quadratic Programming (SQP), Mixed-integer Linear Programming (MILP), Lyapunov-design based nonlinear optimisation control allocation method, direct nonlinear allocation etc. Optimal solutions of Linear Programming (LPs) are found at vertices of the feasible set thereby favouring the use of a smaller number of effectors, while methods based on a quadratic cost function and ∞-norm tend to use all effectors but to a smaller degree [1]. Consider a control allocation scheme and linear effector mapping with an architecture shown in Fig. 1.

The control allocation scheme $\mathbf{K}_{\text{ca}}$ ensures that the forces and moments vector, $\boldsymbol{\tau}$, that characterizes the physical model given by equation (1) is equal to the virtual control demands output, $\boldsymbol{\tau}_c$, produced by the high-level control law (outer linear controller and inner loop NDI controller) $\mathbf{K}_{\text{ctl}}$. The physical vehicle model consists of an effector/actuator model $\mathbf{B}_{\text{e}}$, thus normally would include low-level actuator controller (e.g. servo controllers), and the virtual controls (generalized forces and moments) $\mathbf{G}$. The focus of this study is on the inverse effector model $\mathbf{K}_{\text{ca}}$ (i.e. control allocation) using the effector/actuator model $\mathbf{B}_{\text{e}}$ and generalized forces and moments $\mathbf{G}$ which forms the vehicle with an assumption that $\mathbf{K}_{\text{ctl}}$ is already designed.

The control allocation $\mathbf{K}_{\text{CA}}$ can be formulated by the following problem:

Problem 1. Given an effector mapping

$$\boldsymbol{\tau}(t) = \mathbf{B}_e \mathbf{u}(t), \tag{1}$$

determine the effector demand vector $\mathbf{u}(t)$ such that

$$\boldsymbol{\tau}(t) = \boldsymbol{\tau}_c(t) \tag{2}$$

subject to

$$\underline{\mathbf{u}} \leq \mathbf{u}(t) \leq \overline{\mathbf{u}} \tag{3}$$

$$|\dot{\mathbf{u}}(t)| \leq \dot{\overline{\mathbf{u}}} \tag{4}$$

Less common is when there is a non-linear mapping relating $\mathbf{u}$ and $\boldsymbol{\tau}$. That is, we have the effector mapping

$$\boldsymbol{\tau}(t) = \mathbf{g}_e(\mathbf{u}(t)). \tag{5}$$

This often arises when there are vectored thrust mechanisms (which can be commanded to produce thrust of varying amplitude and direction in two or three degrees of freedom) in the aircraft, such as tilt-rotors, tilt-wings and some of the various eVTOL configurations that are currently attracting research and investor interest [7,17]. Nonlinear control allocation approaches (including nonlinear programming) reviewed in [15] can be used to solve the nonlinear problem with nonlinear effector mapping as in (5) while linear control allocation approaches can be used to solve the optimisation problem is problem (1)-(3).

The parameterisation of the control input, i.e. the choice of elements of the $\mathbf{u}$ vectors in the model, is sometimes crucial. It is usually desirable to choose the effector mapping such that it has a linear form (such as [43]) as in equation (1) and thus avoiding more complex nonlinear control allocation methods. It is also desirable to transform a nonlinear control allocation problem (such as the nonlinear effector mapping for eVTOL with vectored thrust effectors) into a linear one such that linear classical control allocation approaches can then be used. A simple mechanism known as Discrete Time Allocation to transform a non-linear problem to a linear problem was suggested by [45] and proposed [2,4] for traditional aircraft control surfaces (not VTOL aircraft) by time discretization (numerical linearisation) of small enough steps (performing a first order Taylor expansion of the mapping at that point in the control space at each time step) of the effector mapping.

The parameterisation of the control input leading to a linear effector mapping for Vector thrust devices (with nonlinear effector mapping) can be achieved either by (1) an extended thrust formulation [19,31] decomposing its thrust components on the body axes and treating them as elements of the control input $\mathbf{u}$ as used in Control Allocation Approach 1 later proposed in this work or (2) parameterising the thrust by its amplitude and angles as used in Control Allocation Approaches 2 and 3 later proposed in this work. However, the extended thrust formulation results in a more complicated formulation of actuator saturation and rate limit constraints in the control allocation formulation e.g. [16]. The parameterisation of the thrust by its amplitude and angles (formulation

of controls in polar form) requires linearisation of the nonlinear effector mapping to give a Linear Time Varying (LTV) effector mapping.

Linear control allocation approaches (e.g. Active set methods, interior point Quadratic programming etc. [13,25,27,28]) have lower online computational burden and complexity [32] than nonlinear control allocation approaches employing nonlinear programming. The use of Linear control allocation approaches also simplifies the requirements for fault tolerance and reconfigurability.

Another challenge of the VTOL configuration and a crucial constraint for aerial vehicles with coupled control effectors is thrust control saturation where actuator saturation may lead to undesired behaviour, deterioration of the controller performance and even loss of control in specific flight conditions due to the limited control authority during normal and degraded operation (e.g. actuator limitation or failures). Considering a 3DoF VTOL, with an unprioritized control allocation scheme, it may be that the desired combination of pitching moment together with vertical and forward force is not achievable due to maximum or minimum thrust limitations of the thruster and/or due the maximum deflection limits of the tilting mechanisms. In absence of an adequate (prioritised) control allocation algorithm, it is arbitrary which one (or combination) of the three objectives will be affected. However, for the flight stability of these over-actuated vehicles, it is crucial to apply the full required pitching moment before anything else [22,23,35]. Thereafter, the vertical force for altitude (Heave DoF) control comes in the second place, followed by the forward force for the airspeed (surge DoF) which is the least essential from a safety point of view. Therefore, a control allocation algorithm is needed that prioritizes the control objectives of pitching moment over altitude and vertical speed, and subsequently over forward speed, and that calculates the required thrust levels per rotor accordingly.

Amongst the several linear and nonlinear control allocation approaches and techniques proposed for motion control of over-actuated mechanical systems [6,10,15], some of the control allocation schemes address prioritisation, such as linear programming and quadratic programming while others do not address prioritisation (e.g. ganging, redistributed pseudo-inverse, direct control allocation). Active set linear control allocation methods [10,13,25,27,28] for Quadratic programming (QP) addresses control channel prioritisation and are iterative methods, whereby at each iteration they improve their guess of the optimal active set. Interior point method [13,25,28] for quadratic programming on the other hand though also addresses control channel prioritisation, replaces the inequality constraints with a barrier function that prevents the solution for going into the infeasible region.

Although both active set and interior point QP CA methods determine the optimal solution in a finite number of iterations, the active set methods tend to perform well in control allocation problems, [13], while interior point methods have their advantage for larger-scale problems [28]. Active set methods have the advantage that their initialisation can use the previous sample (known as warm/hot start), which is often a good guess for the optimal solution at the current sample. This generally reduces the number of iterations needed to find the optimal solution. Interior-point methods on the other hand are generally initialized with points near the centre of the feasible region and will always need a minimum number of iterations in order to converge due to the need to reduce the barrier function penalty in several steps. Warm start procedures are therefore difficult to implement for interior-point methods [10]. Quadratic Programming (QP) problems are usually solved using active set methods or interior point methods [13,27,28].

In other to avoid the online computational burden of nonlinear programming, this paper proposes three approaches for transforming a nonlinear control allocation problem as in equation (5) to a linear problem as in equation (1) so that classical linear control allocation approaches reviewed above in [15] can then be used. Active Set Linear Quadratic Programming constrained optimisation algorithm was used as the classical control allocation approach. This paper considers a weighted least squares formulation (weighted, bounded least-squares problem) with a quadratic cost function and a corresponding quadratic optimization problem, solves the problem by making a trade off between the actual input commands $\mathbf{U}$ and the virtual commands $\boldsymbol{\tau}$, a solution of which can be found in a straightforward way in [13,14]. The resulting control allocation approaches are novel real-time prioritised control allocation approaches which addresses the main challenges (limited control authority in some specific flight operation, non-linear effector mapping and over-actuation) of the particular VTOL configuration.

The paper then verifies the approaches using the control architecture and NDI high-level controller (aircraft-level controller) proposed in [7] but on a 3DoF planar VTOL version of the over-actuated vectored thrust canard-planform VTOL 6DoF [18] model shown in Fig. 2. A simple 3DoF planar VTOL model with no aerodynamics is chosen to focus this study on control allocation and so that the model can be analysed using first level control knowledge.

The main contributions of this paper are summarized as follows:

- proposes a novel approach for transforming the nonlinear control allocation problem to a linear one by transferring the non-linearity from the effector mapping to the computation of the actuator limits but formulates the individual effector demand (real controls) in cartesian form (decomposing its thrust components on the body axes) resulting in a Linear Effector mapping. It retains the overall control demands (virtual control) in cartesian form. The required computation of the actuator limits which converts the physical actuator limits from polar to cartesian form is however non-linear and complex. It proposes a more rigorous and analytical solution to the problem of conversion of the actuator limits from polar to cartesian, over the heuristic solution provided by [8,36]. This control allocation approach will be known as CA Approach 1 or Extended Thrust Formulation CA thereafter.
- proposes a novel approach for transforming the nonlinear control allocation problem to a linear one by transforming the effector mapping from non-linear to linear via linearisation of the non-linear effector mapping in real-time resulting in a Linear Time Varying (LTV) effector mapping (control effectiveness matrix - Jacobian of $\boldsymbol{\tau}$ with respect to $\mathbf{u}$) with the real controls formulated in incremental polar form. This control allocation approach will be known as CA Approach 2 thereafter.
- proposes another approach for transforming the nonlinear control allocation problem to linear one which is similar to CA Approach 2 above except an extra step which transforms the virtual controls from cartesian to polar before differentiation and linearisation resulting in a different and more complicated LTV Effector mapping. This control allocation approach will be known as CA Approach 3 thereafter.
- compares the performance of all three control allocation approaches (CA Approach 1, CA Approach 2 and CA Approach 3) for three unusual flight manoeuvres (aircraft control manoeuvres) which may be different from how an aircraft is normally flown. The choice of the two selected manoeuvres is to enable analysis of the CA performance during limited control authority due to actuator saturation in the absence of any aerodynamic lift and drag being a planar VTOL. The selected aircraft control manoeuvres are:
  - VTO/VL with pitch control and limited control authority.
  - Reverse and pitch control with limited control authority

Table 1 shows a summary comparison of the three control allocation approaches features.

The rest of this paper is structured as follows: the 3DoF equations of motion and vehicle dynamic model, a summary of the control architecture and high-level control laws, and General control allocation concepts and the proposed classical/linear control allocation technique are presented in sections 2.1, 2.2 and 2.3 respectively. Control Allocation Approach 1 is presented in section 3, Control Allocation Approach 2 is presented in section 4 while Control Allocation Approach 3 is presented in section 5. The nonlinear control simulations results of some

Table 1
Control Allocation Approaches Comparison.

CA Approaches	$\boldsymbol{\tau}_c$ form	**u** form	Eff. Map	Eff. Const.	CA	Coupled Thrust
Approach 1	Abs Cart	Abs Cart	linear	Pol to Cart	AS - Abs	No
Approach 2	Incr Cart	Incr Pol	Num., LTV	Abs to Incr	AS - Incr	Yes
Approach 3	Incr Pol	Incr Pol	Ana., LTV	Abs to Incr	AS - Incr	+Approach 2 Yes

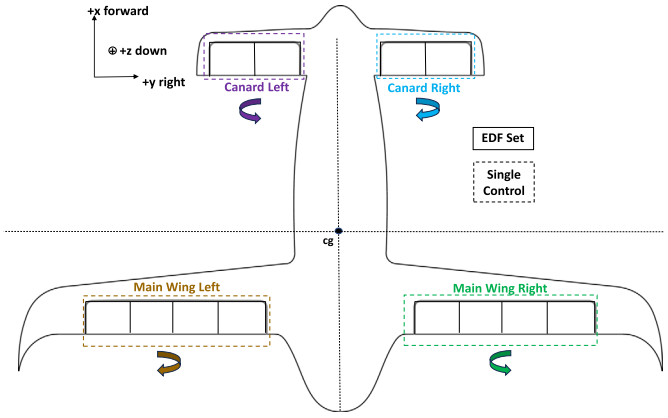

Fig. 2. Plan View of Over-actuated Vectored Thrust Canard-planform 6DoF VTOL aircraft showing EDF sets distribution.

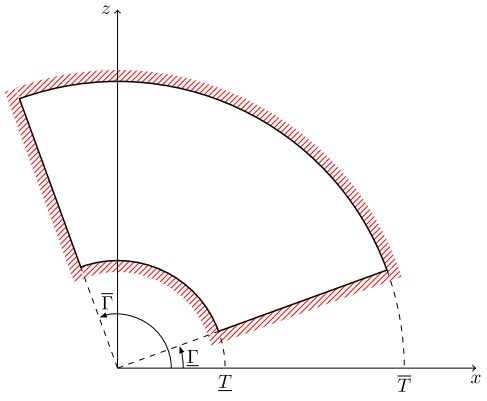

Fig. 3. Vectored Thrust Actuator Limits Illustration.

selected manoeuvres are presented and analysed in section 6. In the final section 7, the proposed CA solutions are discussed as well as any limitations and future work.

2. Vehicle model, NDI controller and classical control allocation

2.1. Vehicle dynamic model

The vehicle model of an over-actuated canard-planform vectored thrust VTOL vehicle whose 6DoF version is shown in Fig. 2, which also shows the EDF arrangement whereby the fans are ganged together in sets of three. Multirotor models are relatively complicated, hence some insight can be obtained by restricting the vehicle motion to the vertical plane. The vehicle then has just three degrees-of-freedom, so the models are simple and can be analysed using first level control knowledge. Hence a 3DoF planar VTOL model similar to the VTOL aircraft studies [9,40,41] is chosen.

The vectored thrust actuator (thrust T and tilt angle Γ) limits are illustrated in Fig. 3 which only shows the actuator position limits for simplicity. The unshaded regions are the set of admissible controls U constrained by the effector limits. The physical/polar position and rate limits of the actuator thrust and tilting mechanism are as follows:

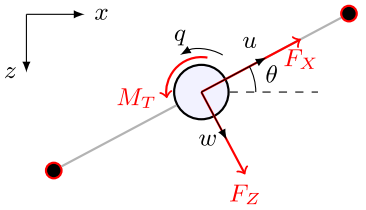

Fig. 4. 3DoF motion showing aircraft state variables and virtual controls.

- *Actuator Thrust position limit:* $\overline{T}$, $\underline{T}$
- *Actuator Thrust rate limit:* $\dot{\overline{T}}$, $\dot{\underline{T}}$
- *Tilting mechanism position limits:* $\overline{\Gamma}$, $\underline{\Gamma}$
- *Tilting mechanism rate limits:* $\dot{\overline{\Gamma}}$, $\dot{\underline{\Gamma}}$

2.1.1. 3DoF mathematical model

Considering 3DoF longitudinal motion, surge, heave and surge, the equations of motion are:

$$\dot{u} = \frac{1}{m} F_X - g \sin\theta - qw \tag{6}$$

$$\dot{w} = \frac{1}{m} F_Z + g \cos\theta + qu \tag{7}$$

$$\dot{q} = \frac{1}{I_{yy}} M_T \tag{8}$$

$$\dot{\theta} = q \tag{9}$$

$$\dot{x} = u \cos\theta + w \sin\theta \tag{10}$$

$$\dot{z} = w \cos\theta - u \sin\theta \tag{11}$$

The 3DoF schematic is shown in Fig. 4. The longitudinal state variable vector $\mathbf{x}$ and virtual control vector $\boldsymbol{\tau}$ are respectively given by:

$$\mathbf{x} = \begin{bmatrix} u & w & q & \theta & x & z \end{bmatrix}^T \tag{12}$$

$$\boldsymbol{\tau} = \begin{bmatrix} F_X & F_Z & M_T \end{bmatrix}^T \tag{13}$$

2.2. Control design

The controller structure/architecture and the high-level controller (Classical NDI) is that presented in [7] hence will only be outlined here since it is not the focus of this study.

2.2.1. Control architecture

The control architecture is shown in Fig. 5. The controller comprises a high-level controller (control law) and the control allocation. The higher-level controller consists of an outer-loop position controller and an inner loop velocity controller. A hard switch is used to switch between velocity and position control. In velocity control mode the references are pitch attitude θ_r, airspeed V_r and flight path angle λ_r. These are controlled directly by the NDI inner-loop feedback. For position control mode, the references are pitch attitude θ_r, lateral position x_r and altitude h_r.

2.2.2. NDI control law

Consider a plant model with general state equations given by:

$$\dot{\mathbf{x}} = \mathbf{f}(\mathbf{x}) + \mathbf{g}(\mathbf{x})\boldsymbol{\tau}_c \tag{14}$$

$$\mathbf{y} = \mathbf{h}(\mathbf{x}) \tag{15}$$

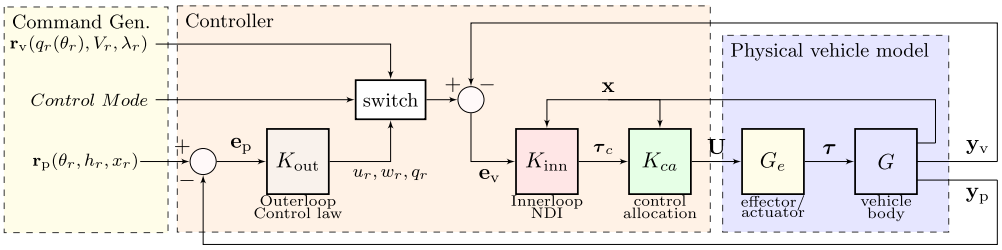

Fig. 5. Generic Flight Control Architecture for piloted, semi-automatic and automated flight [7].

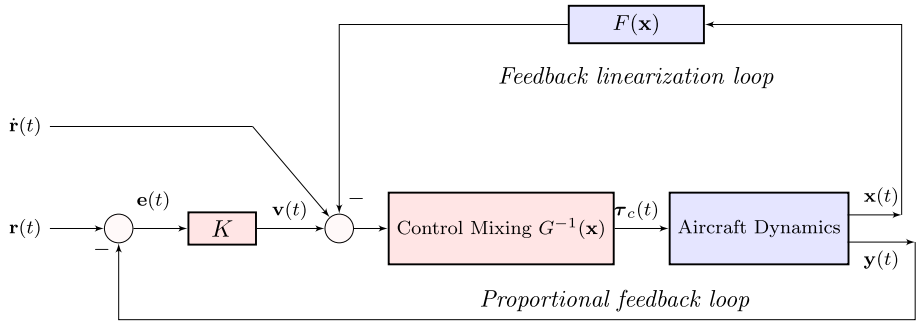

Fig. 6. NonLinear Dynamic Inversion (NDI) problem formulation [7].

where $\mathbf{x}(t) \in \mathbb{R}^n$ is the vector of state variables, $\boldsymbol{\tau}_c \in \mathbb{R}^m$ is the (virtual) control, $\mathbf{y}(t) \in \mathbb{R}^m$ is the vector of outputs to be controlled and the error is given by:

$$\mathbf{e}(t) = \mathbf{r}(t) - \mathbf{y}(t) \tag{16}$$

where $\mathbf{r}(t) \in \mathbb{R}^m$.

Based on the exposition in [7,33], the NDI controller is

$$\mathbf{v} = \mathbf{K}\mathbf{e} \tag{17}$$

$$\boldsymbol{\tau}_c = \mathbf{G}^{-1}(\mathbf{x})\left[-\mathbf{F}(\mathbf{x}) + \dot{\mathbf{r}} + \mathbf{v}\right] \tag{18}$$

where

$$\mathbf{F}(\mathbf{x}) := \frac{\partial \mathbf{h}}{\partial \mathbf{x}}\mathbf{f}(\mathbf{x}), \qquad \mathbf{G}(\mathbf{x}) := \frac{\partial \mathbf{h}}{\partial \mathbf{x}}\mathbf{g}(\mathbf{x}) \tag{19}$$

and $\mathbf{v}$ ensures that $\mathbf{v} = \mathbf{K}\mathbf{e}$

The controller structure is shown in Fig. 6 and consists of the linear output feedback loop equations (17) and the state feedback linearisation loop (with linear controller $\mathbf{K}$ in equation (18)) which assumes all the states are observable. The feedback linearisation loop ensures that the system from $\mathbf{v}(t)$ to $\mathbf{y}(t)$ appears like a linear system with poles at the origin, thus simplifying the outer tracking loop design. The velocity feedforward term $\dot{\mathbf{r}}$ improves the tracking accuracy of the closed-loop system. This signal is generated either by the pilot inceptor for manned operation or the guidance system for automated flight.

Since the controller in Fig. 6 contains a model of the aircraft dynamics (equation (19)), the nonlinear functions of the aircraft must be known in order to implement it. The classical NDI inner loop is airframe-dependent, uses an onboard (OBM) model of aircraft to invert and cancel the airframe dynamics such that the system appears as an integrator. The outer NDI loop is airframe-independent and can also be used for flying and handling quality control design. Refer to [7] for classical NDI controller details applied in this work.

2.2.3. Outer-loop linear controller

As stated in [5], to control the uncontrolled states, the controllable states can be used as the controls resulting in a cascaded loop consisting of the inner controllable state variables (u, w, q) velocity loop (section 2.2.2 above) and an outer uncontrolled state variables (x, z, θ) position loop. A simple diagonal proportional (P) linear controller is used for the outer loop control. The outer-loop linear controller $\mathbf{K}_{\text{out}}$ consists of the following:

- Altitude ($h = -z$) controller - PI Controller
- Pitch attitude (θ) controller - P Controller
- Position (x) controller - PI Controller

2.3. General control allocation

The classical control allocation problem is to map a vector of virtual control demands $\boldsymbol{\tau}_c \in \mathbb{R}^{\ell}$ to a vector of effector positions/actuator demands $\mathbf{u} \in \mathbb{R}^p$ where $\ell \leq p$. In the classical problem [6] there is a known linear relationship between $\mathbf{u}$ and $\boldsymbol{\tau}$, that is $\boldsymbol{\tau}_c = \mathbf{B}_e\mathbf{u}$ where $\boldsymbol{\tau}_c$ is the virtual control input in the system model, usually in the form of a vector of generalized forces and moments. The problem is then to determine the effector/actuator demand vector $\mathbf{u}$ such that $\boldsymbol{\tau} = \boldsymbol{\tau}_c$ with the constraint $\boldsymbol{\tau} = \mathbf{B}_e\mathbf{u}$. The scheme is illustrated in Fig. 1. If $\ell = p$ then the solution is trivially given by $\mathbf{u} = \mathbf{B}_e^{-1}\boldsymbol{\tau}_c$ (for example the quadrotor control problem) under the assumption that $\mathbf{B}_e$ is full rank and that no effector constraints are breached. If $\ell > p$ then multiple solutions exist, for example $\mathbf{u} = \mathbf{B}_e^{\dagger}\boldsymbol{\tau}_c$ where $[\cdot]^{\dagger}$ represents the Moore-Penrose inverse of the matrix. Hence the problem is often extended to account for some other requirements (e.g. minimum power) as well as to take account of various constraints. The constraints are for example saturation constraints on $\mathbf{u}$ and slew rate constraints on $|\dot{\mathbf{u}}|$.

2.3.1. Control allocation formulation

As mentioned in the previous section, minimising the control error ($\mathbf{s} = \boldsymbol{\tau}_c - \mathbf{B}_e(\mathbf{u}, \mathbf{x}, t)$) known as a primary objective or equality constraints, imposing additional physical constraints in form of affector/actuator saturation and rate limits (inequality constraints), and introduction of secondary objective(s) (e.g. control minimisation) to the control allocation algorithm ensuring a unique solution results in the following control allocation formulation:

$$\begin{aligned} \min_{\mathbf{u}\in\mathbb{R}^p, \mathbf{s}\in\mathbb{R}^m} \quad & \left(\|W_v s\| + J(\mathbf{x}, \mathbf{u}, t)\right) \text{ s.t.} \\ & \boldsymbol{\tau} - \mathbf{B}_e(\mathbf{u}, \mathbf{x}, t) = \mathbf{s}, \mathbf{u} \in \mathbf{U}, \mathbf{u} = \mathbf{u}_l + \Delta\mathbf{u}, \Delta\mathbf{u} \in \mathbf{C} \end{aligned} \tag{20}$$

$$J(\mathbf{x}, \mathbf{u}, t) = \frac{1}{2}(\mathbf{u} - \mathbf{u}_p)^T \mathbf{W}_u (\mathbf{u} - \mathbf{u}_p) \tag{21}$$

$$J(\mathbf{x},\mathbf{u},t) = \left\|\mathbf{W}_u\mathbf{u}\right\| \tag{22}$$

2.3.2. Active set prioritised constrained linear control allocation

Due to the advantages (perform well in control allocation problems, can be warm-started) of Active set over Interior point QP CA method [13,28], Active Set QP CA is selected for this work. Some Active set QP formulations are Weighted Least Squares (WLS), Sequential Least Squares (SLS) and Minimal Least Squares (MLS). For this work, a 2-norm quadratic program (QP) formulation known as weighted Least Squares that can be solved using numerical QP methods, e.g. [13,27,28] is chosen. Throughout this work, the classical linear control allocation algorithm is an online/real-time constrained optimisation based on the Active Set Linear QP algorithm [13,14] with a novel functional architecture generic for piloted, semi-automatic and automated flight based on [7].

The MATLAB® toolbox QCAT [12] QP-based control allocation, an implementation of the methods in [13,28] was customised for use in this work.

The active set algorithm solves the bounded and equality constrained least squares problem by solving a sequence of equality constrained problems. In each step, some of the inequalities are regarded as equality constraints, and form the working set *W*, while the remaining inequality constraints are disregarded. The control allocation method uses a dynamic model where the resulting control distribution depends not only on the current control virtual demand but also on the distribution in the previous sampling instant due to the actuator rate limit constraints. The control allocation problem is posed as a constrained quadratic programming problem which provides automatic redistribution of the control effort when one actuator saturates in position or in rate.

As discussed in section 1, Active set linear control allocation methods [10,13,25,27,28] for Quadratic programming (QP) addresses control channel prioritisation using the value of $\mathbf{W}_v$ in equation (82) to overcome a major challenge and crucial constraint for the vectored thrust eVTOL configuration of thrust control saturation due to actuator saturation with a potential to lead to undesired behaviour, deterioration of the controller performance and even loss of control in specific flight conditions due to the limited control authority during normal and degraded operation (e.g. actuator limitation or failures). Other parameters for the prioritised constrained linear optimisation Active Set algorithm are listed in Table 4 with detailed explanation presented in section 6.

3. Control Allocation Approach 1 - extended thrust formulation

One of the main contributions of this work is the design of a novel control allocation architecture and approach for transforming the non-linear control allocation problem for vectored thrust VTOL with non-linear effector mapping to a linear problem by transferring the non-linearity from the effector mapping to the computation of the actuator limits as stated in section 1 known as CA Approach 1 or Extended thrust formulation CA. It retains the overall control demands (virtual control) in cartesian form but formulates the individual effector demand (real controls) in cartesian form (decomposing its thrust components on the body axes) resulting in a Linear Effector mapping allowing the use of classical linear control allocation techniques with prioritisation. The required computation of the actuator limits which converts the physical actuator limits from polar to cartesian form is however non-linear and complex offering a more rigorous and analytical solution to the problem of conversion of the actuator limits from polar to cartesian, an improvement over [8,35,36] whereby the solution is heuristics in nature. This control approach offers a real-time analytical optimal control allocation (i.e., does not utilize optimization software and linearized effector model – control effectiveness matrix) which considers both actuator saturation and rate limits using active set Prioritised linear QP Weighted Least squares (WLS) formulation as the linear control allocation algorithm. The computation of the actuator limits uses the physical (polar) actuator limits, the previous cycle value of the real controls in cartesian form and the previous cycle value of the real controls in polar form.

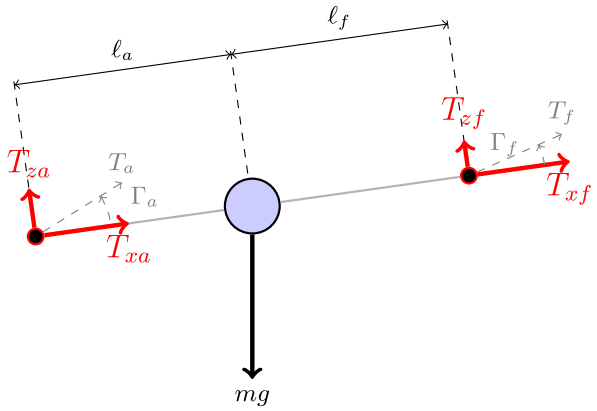

Fig. 7. CA Approach 1 - 3DoF VTOL schematic showing effector variables.

3.1. CA Approach 1 - formulation of real controls resulting in a Linear Effector mapping

The 3DoF aircraft model showing the effector model is shown in Fig. 7.

The effectors are a canard (fore) and main wing (aft) pair of decoupled thrust components along the body x and z axes T_{xf} and T_{xa}, T_{zf} and T_{za} respectively as shown in Fig. 7. Formulating the vector of real controls in cartesian form as:

$$\mathbf{u}_{x,z} = \begin{bmatrix} T_{xf} & T_{xa} & T_{zf} & T_{za} \end{bmatrix}^T, \tag{23}$$

and the generalised forces and moments (commanded virtual controls τ) as:

$$\boldsymbol{\tau}_c = \begin{bmatrix} F_X & F_Z & M_T \end{bmatrix}^T \tag{24}$$

The effector mapping is given by:

$$\begin{bmatrix} F_X \\ F_Z \\ M_T \end{bmatrix} = \begin{bmatrix} 1 & 1 & 0 & 0 \\ 0 & 0 & -1 & -1 \\ 0 & 0 & \ell_c & \ell_w \end{bmatrix} \begin{bmatrix} T_{xf} \\ T_{xa} \\ T_{zf} \\ T_{za} \end{bmatrix} \tag{25}$$

Such that the effector model equation is of the form in equation (1) and is given below:

$$\boldsymbol{\tau}_c = \mathbf{B}_u(\mathbf{x},t)\mathbf{u}_{x,z} \tag{26}$$

where

$$\mathbf{B}_u(l_a,l_f) = \begin{bmatrix} 1 & 1 & 0 & 0 \\ 0 & 0 & -1 & -1 \\ 0 & 0 & \ell_f & \ell_a \end{bmatrix}. \tag{27}$$

3.2. CA Approach 1 functional architecture

The control allocation architecture is shown in Fig. 8 and consist of four parts:

- *Step 1 - Formulation of real controls in cartesian form resulting in a linear effector mapping*
- *Step 2 - Transformation of previous cycle real controls from cartesian to polar form*
- *Step 3 - Conversion of the actuator constraints from polar to cartesian*
- *Step 4 - Application of prioritised linear control allocation technique*

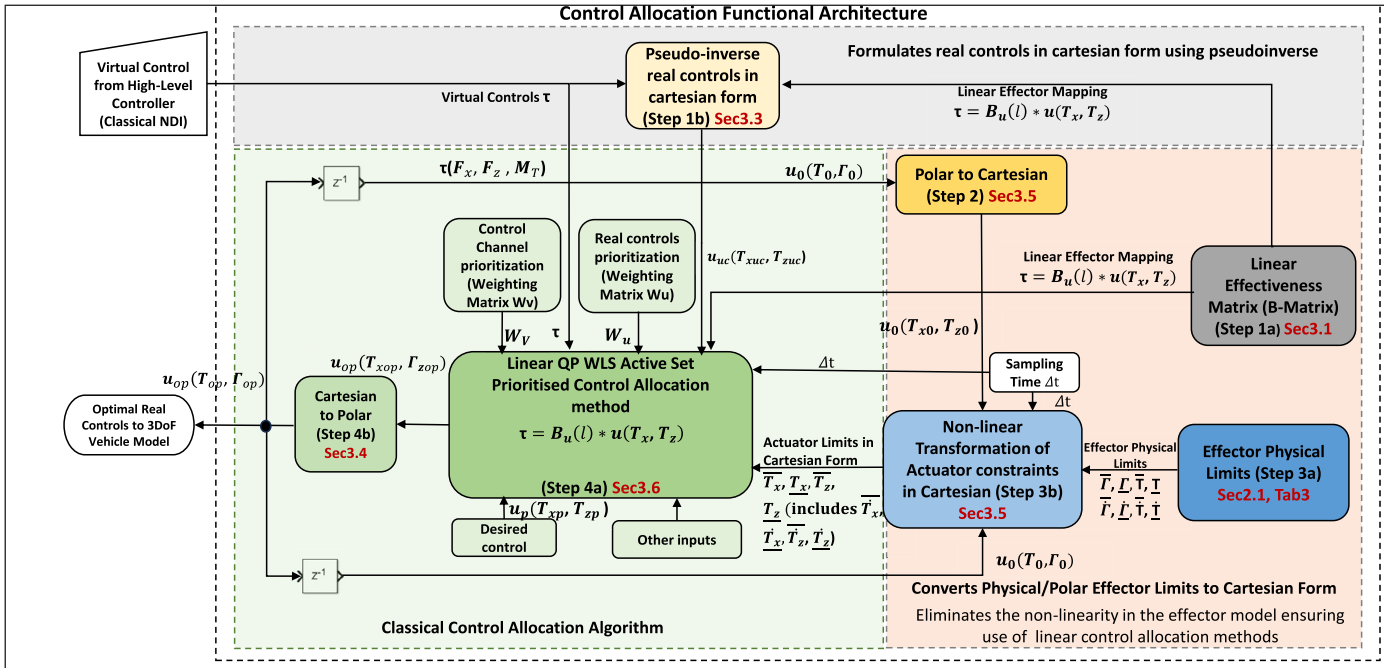

Fig. 8. CA Approach 1 Functional Architecture.

3.3. Computation of unconstrained controls

The unconstrained real control is given by the Moorse-Penrose pseudo-inverse:

$$\mathbf{u}_{x,z} = \mathbf{B}_{\mathbf{u}}^{+}(l_a, l_f)\boldsymbol{\tau}_c \tag{28}$$

where:

$$\mathbf{B}_{\mathbf{u}}^{+}(\mathbf{x}, t) = \mathbf{B}_u(l_a, l_f)^T(\mathbf{B}_u(l_a, l_f)\mathbf{B}_u(l_a, l_f)^T)^{-1} \tag{29}$$

3.4. Transformation of previous cycle real controls from cartesian to polar form

The previous cycle real controls in polar form are given by:

$$T_0 = \sqrt{(T_{x0}{}^2 + T_{z0}{}^2)} \tag{30}$$

$$\Gamma_0 = \arctan 2\,(T_{z0}, T_{x0}) \tag{31}$$

3.5. Conversion of actuator limits from polar to Cartesian

Given a vectored thrust actuator which can produce thrust T (N) which can be oriented at an angle Γ (rad) to the body x-axis within the body x-z plane subject to position and rate limit shown in Fig. 3 in Section 2.

Decoupling the actuator thrust (T (N) oriented at an angle Γ (rad)) into body x and z components assuming NEU convention, we have:

$$T_x = T\cos(\Gamma) \tag{32}$$

$$T_z = T\sin(\Gamma) \tag{33}$$

Linearizing with small perturbations we get the Jacobian matrix:

$$\begin{bmatrix}\Delta T_x \\ \Delta T_z\end{bmatrix} = \begin{bmatrix}\cos\Gamma_0 & -T_0\sin\Gamma_0 \\ \sin\Gamma_0 & T_0\cos\Gamma_0\end{bmatrix}\begin{bmatrix}\Delta T \\ \Delta\Gamma\end{bmatrix} \tag{34}$$

Expanding equations (34) gives:

$$\Delta T_x = \Delta T\cos\Gamma_0 - \Delta\Gamma T_0\sin\Gamma_0 \tag{35}$$

$$\Delta T_z = \Delta T\sin\Gamma_0 + \Delta\Gamma T_0\cos\Gamma_0 \tag{36}$$

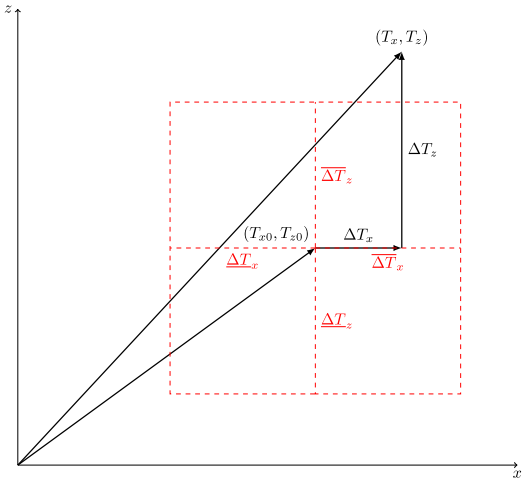

Fig. 9. Combined Position and rate Cartesian Limits Illustration.

Considering all the combinations of minimum and maximum thrust (T) and tilt angle (Γ) limits in equations (35), (36) and:

$$T_x = T_{x0} + \Delta T_x \tag{37}$$

$$T_z = T_{z0} + \Delta T_z \tag{38}$$

then the combined position and rate actuator limits in cartesian form illustrated in Fig. 9 are given by:

$$\underline{T}_x = \min(T_{x\underline{T}\underline{\Gamma}}, T_{x\underline{T}\overline{\Gamma}}, T_{x\overline{T}\underline{\Gamma}}, T_{x\overline{T}\overline{\Gamma}}) \tag{39}$$

$$\overline{T}_x = \max(T_{x\underline{T}\underline{\Gamma}}, T_{x\underline{T}\overline{\Gamma}}, T_{x\overline{T}\underline{\Gamma}}, T_{x\overline{T}\overline{\Gamma}}) \tag{40}$$

$$\underline{T}_z = \min(T_{z\underline{T}\underline{\Gamma}}, T_{z\underline{T}\overline{\Gamma}}, T_{z\overline{T}\underline{\Gamma}}, T_{z\overline{T}\overline{\Gamma}}) \tag{41}$$

$$\overline{T}_z = \max(T_{z\underline{T}\underline{\Gamma}}, T_{z\underline{T}\overline{\Gamma}}, T_{z\overline{T}\underline{\Gamma}}, T_{z\overline{T}\overline{\Gamma}}) \tag{42}$$

where

$$T_{x\underline{T}\underline{\Gamma}} = T_{x0} + \underline{\Delta T}\cos\Gamma_0 - \underline{\Delta\Gamma} T_0\sin\Gamma_0 \tag{43}$$

$$T_{x\underline{T}\overline{\Gamma}} = T_{x0} + \underline{\Delta T}\cos\Gamma_0 - \overline{\Delta\Gamma}T_0\sin\Gamma_0 \tag{44}$$

$$T_{x\overline{T}\underline{\Gamma}} = T_{x0} + \overline{\Delta T}\cos\Gamma_0 - \underline{\Delta\Gamma}T_0\sin\Gamma_0 \tag{45}$$

$$T_{x\overline{T}\overline{\Gamma}} = T_{x0} + \overline{\Delta T}\cos\Gamma_0 - \overline{\Delta\Gamma}T_0\sin\Gamma_0 \tag{46}$$

$$T_{z\underline{T}\underline{\Gamma}} = T_{z0} + \underline{\Delta T}\sin\Gamma_0 + \underline{\Delta\Gamma}T_0\cos\Gamma_0 \tag{47}$$

$$T_{z\underline{T}\overline{\Gamma}} = T_{z0} + \underline{\Delta T}\sin\Gamma_0 + \overline{\Delta\Gamma}T_0\cos\Gamma_0 \tag{48}$$

$$T_{z\overline{T}\underline{\Gamma}} = T_{z0} + \overline{\Delta T}\sin\Gamma_0 + \underline{\Delta\Gamma}T_0\cos\Gamma_0 \tag{49}$$

$$T_{z\overline{T}\overline{\Gamma}} = T_{z0} + \overline{\Delta T}\sin\Gamma_0 + \overline{\Delta\Gamma}T_0\cos\Gamma_0 \tag{50}$$

and where the incremental physical/polar actuator limits are given by;

$$\overline{\Delta T} = \min((\overline{T} - T_0), (\dot{\overline{T}}\Delta t)) \tag{51}$$

$$\underline{\Delta T} = \max((\underline{T} - T_0), (\dot{\underline{T}}\Delta t)) \tag{52}$$

$$\overline{\Delta\Gamma} = \min((\overline{\Gamma} - \Gamma_0), (\dot{\overline{\Gamma}}\Delta t)) \tag{53}$$

$$\underline{\Delta\Gamma} = \max((\underline{\Gamma} - \Gamma_0), (\dot{\underline{\Gamma}}\Delta t)) \tag{54}$$

where Δt is the iteration period of the control allocation module, T_0 and Γ_0 are respectively the thrust and actuator tilt angle at the initial or previous iteration, $\overline{T}$, $\underline{T}$, $\dot{\overline{T}}$, $\dot{\underline{T}}$ are respectively the physical thrust saturation and rate limits, and $\overline{\Gamma}$, $\underline{\Gamma}$, $\dot{\overline{\Gamma}}$, $\dot{\underline{\Gamma}}$ are respectively the physical tilting mechanism actuator angle saturation and rate limits.

3.6. CA Approach 1 - prioritised linear control allocation

To solve the CA problem in equation (20) following the active set described in [13], the problem is first formulated in weighted least squares form given by:

$$\mathbf{u}_{op} = \arg\min_{\underline{\mathbf{u}}\le u\ge\bar{\mathbf{u}}} \left\|\mathbf{W}_u(\mathbf{u}-\mathbf{u}_p)\right\|^2 + \gamma\left\|\mathbf{W}_v(\mathbf{B}\mathbf{u}-\boldsymbol{\tau})\right\|^2 \tag{55}$$

The cost function is incorporated in ***Algorithm 1*** given below as follows:

Algorithm 1 - CA Approach 1 WLS formulation for Active Set [13].

1. Let $\mathbf{u}^0$ and $\mathbf{W}$ be the optimal solution and working set respectively from the previous sampling instant.
2. Rewrite the cost function as:

$$\left\|\mathbf{W}_u(\mathbf{u}-\mathbf{u}_p)\right\|^2 + \gamma\left\|\mathbf{W}_v(\mathbf{B}\mathbf{u}-\boldsymbol{\tau})\right\|^2 = \left\|\begin{pmatrix}\gamma\mathbf{W}_v\mathbf{B}\\ \mathbf{W}_u\end{pmatrix}\mathbf{u} - \begin{pmatrix}\gamma\mathbf{W}_v\boldsymbol{\tau}\\ \mathbf{W}_u\mathbf{u}_p\end{pmatrix}\right\|^2$$

3. and solve

$$\mathbf{u}_{op} = \arg\min_{\underline{\mathbf{u}}\le\mathbf{u}\le\bar{\mathbf{u}}} \left\|\mathbf{A}_{as}\mathbf{u} - \mathbf{q}\right\|$$

using ***Algorithm 2*** where:

$$\mathbf{A}_{as} = \begin{pmatrix}\gamma\mathbf{W}_v\mathbf{B}\\ \mathbf{W}_u\end{pmatrix} \tag{56}$$

$$\mathbf{q} = \begin{pmatrix}\gamma\mathbf{W}_v\mathbf{v}\\ \mathbf{W}_u\mathbf{u}_p\end{pmatrix} \tag{57}$$

4. NOTE: The weighted rows are ordered first in $\mathbf{A}_{as}$ (row augumented weighted virtual control matrix) and $\mathbf{q}$ (row augumented weighted real control matrix) to avoid numerical problems.

The Active Set algorithm (***Algorithm 2***) is presented below.

4. Control Allocation Approach 2

As stated in section 1, a second contribution of this work is the proposal of another approach (Control Allocation Approach 2) which is a simple mechanism to transform non-linear problems to linear problems similar to that suggested by [45] and in the work of [2,4] for traditional flight control surfaces. This is done by a time discretization (numerical linearisation) of small enough steps to ensure the linearization step is accurate. At each time-step, a first order Taylor expansion of the mapping at that point in the control space (in a similar manner to an Extended Kalman Filter [11, pp. 374]). Classical control allocation can then be applied and the constraints satisfied. The resulting point in the effector space is tracked and the process repeated at each time-step. Again the scheme relies on the feedback control of the system to account for uncertainty in the linearization and effector-control mappings. Sometimes the effector forces and moments depend on the system state $\mathbf{x}(t) \in \mathbb{R}^n$ as well as the effector controls.

Algorithm 2 - CA Approach 1 Active Set Algorithm [13].

1. Let $\mathbf{u}^0$ be a feasible starting point. A point is feasible if it satisfies both the control constraint ($\mathbf{B}\mathbf{u} = \mathbf{v}$) and actuator constraints ($\underline{\mathbf{u}} \le \mathbf{u} \le \bar{\mathbf{u}}$).
2. Let the working set $\mathbf{W}$ contain (a subset of) the active inequality constraints at $\mathbf{u}^0$
3. **for** $k = 0, 1, 2..., N-1$ **do**
4. Given $\mathbf{u}^k$ the value of $\mathbf{u}$ at the k^{th} step, find the optimal perturbation $\mathbf{p}$, considering the constraints in the working set $\mathbf{W}$ as equality constraints and disregarding the remaining inequality constraints. Solve

$$\min_{\mathbf{q}} \left\|\mathbf{A}(\mathbf{u}_k + \mathbf{p}) - \mathbf{q}\right\| \quad \mathbf{B}\mathbf{p} = 0 \quad \mathbf{p}_i = 0, i \in \mathbf{W} \tag{58}$$

where $\mathbf{A}_{as}$ and $\mathbf{q}$ are as defined in equations (56) and (57)

5. **if** $\mathbf{u}^k + \mathbf{p}$ is feasible **then**
6. Set $\mathbf{u}^{k+1} = \mathbf{u}^k + \mathbf{p}$ and compute the Lagrange multipliers, $\begin{pmatrix}\boldsymbol{\mu}\\ \lambda\end{pmatrix}$, where $\boldsymbol{\mu}$ and λ are associated with the control constraint ($\mathbf{B}\mathbf{u} = \mathbf{v}$) and actuator constraints ($\underline{\mathbf{u}} \le \mathbf{u} \le \bar{\mathbf{u}}$) respectively
7. **if** all elements of $\lambda \ge 0$ **then**
8. $\mathbf{u}_{op} = \mathbf{u}^{k+1}$ is the optimal solution to equation (58)
9. **else**

Remove the constraint associated with the most negative λ from the working set

10. **else**

Determine the maximal step length α such that α such that $\mathbf{u}^{k+1} = \mathbf{u}^k + \alpha\mathbf{p}$ is feasible. Add the primary bounding constraint to the working set.

11. **end**

Although for this system, the rotor thrust for a particular rotor rotational speed depends on the air density which in turn is dependent on altitude (an aircraft state), for simplicity and since the thrust (rather than the rotation speed or RPM) is used as the real control changes in air density over the altitude range of the VTOL are ignored. In reality, for this kind of VTOL configuration where there are aerodynamic couplings with the propulsive forces such as that studied in [24] where the total 3DoF/longitudinal virtual forces/generalised forces and moment (net forward thrust/drag, lift and pitching moment) are a complex (3D) function of the controls $\mathbf{u}$ (fan power/RPM, tilt angle Γ) and states $\mathbf{x}$ (AoA α and airspeed V), (62) can be used but the jacobians (differentials) of the virtual forces with respect to the states (α, V) and controls (RPM, Γ) have to be computed offline numerically and stored onboard aircraft as complex 3D lookup tables as stated in [2] for the case of traditional aircraft control surfaces. This is outside the scope of this study and is recommended as future studies.

The functional architecture is shown in Fig. 11. It converts the overall control demands (virtual control) from absolute cartesian to incremental cartesian form before the numerical linearisation of the nonlinear effector mapping to a Linear Time Varying (LTV) effector mapping. Since the real controls are formulated in polar form it requires only a transformation of the actuator limits from absolute to incremental polar form. It offers a real-time analytical optimal control allocation which considers both actuator saturation and rate limits using active set Prioritised linear QP Weighted Least squares (WLS) formulation as the linear control allocation algorithm.

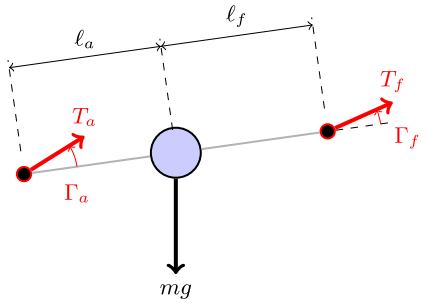

Fig. 10. 3DoF VTOL schematic showing the effector variables for CA Approaches 2 and 3.

However, since the virtual controls input to the control allocation are differentiated to give discretised (incremental) values to enable dynamic computation of the Linear Time Varying (LTV) effector mapping with an incremental polar real controls output from the algorithm before being reintegrated again to give the controls, this scheme is prone to drift in the presence of noise in either the differentiated virtual controls or the CA incremental output. Also, it is prone to drift because the CA algorithm computes only the change in control and unable to track the reference due to the control allocation being open loop in terms of system states despite being closed loop in terms of the effector positions because the current control is a function of the previous actuator positions.

To correct the drift, we proposed similar approaches used in Kalman filter (KF) and Extended Kalman Filter (EKF) [11, pp. 374] to update the estimate/prediction using measurement from another source which doesn't drift (often a slower and less noiser source). We propose a complementary filter (with static gain) unlike the KF and EKF where the Kalman Gain is dynamic and varies depending on errors in estimation and measurement. The choice of a simple complementary filter is made because the characteristics of the noise which is due to differences (unable to track changes) in unconstrained and constrained control allocation ouputs (changes in real controls) during actuator saturation are not zero-mean gaussian - a major prerequisite/assumptions for use of Kalman Filter. The main incremental CA outputs is the estimate/prediction while the differentiated non-incremental (absolute) CA output sources is selected as the measurement/update. Without this drift correction via a complementary filter, the CA output will drift after actuator saturation resulting in a steady state error in the system states in a similar fashion to insufficient integration action in the control laws.

4.1. CA Approach 2 effector model formulation

The effectors (real controls) in polar form are fore and aft pair of vectored thrusters with thrust T_f and T_a acting at angles Γ_f and Γ_a respectively as shown in Fig. 10.

The control forces and moment (overall control demand or virtual controls) are thus given by

$$T_X = T_f \cos\Gamma_f + T_a \cos\Gamma_a, \tag{59}$$

$$T_Z = -T_f \sin\Gamma_f - T_a \sin\Gamma_a, \tag{60}$$

$$M_T = -T_f \ell_f \sin\Gamma_f + T_a \ell_a \sin\Gamma_a, \tag{61}$$

where ℓ_f and ℓ_a are the front and aft thrusters moment arms respectively.

Defining the virtual forces and moment control vector as $\boldsymbol{\tau}_c = \begin{bmatrix} F_X, & F_Z, & M_T \end{bmatrix}^T$ and the real control vector as $\mathbf{u} = \begin{bmatrix} T_f, & T_a, & \Gamma_f, & \Gamma_a \end{bmatrix}^T$ we get the nonlinear mapping $\boldsymbol{\tau}_c(t) = \mathbf{g}_e(\mathbf{u}(t))$ defined by equations (59)–(61).

4.2. CA Approach 2 functional architecture

The control allocation architecture is shown in Fig. 11 and consist of five steps:

- *Step 1 - Computation of the actuator incremental limits at each time step*
- *Step 2 - Linearization of the nonlinear effector mapping to linear-time-varying effector mapping*
- *Step 3 - Discretisation of virtual controls and computation of unconstrained real controls*
- *Step 4 - Application of classical constrained linear control allocation technique*
- *Step 5 - Correction of drift using complementary filter*

4.3. Control allocation incremental constraints formulation

The incremental actuator limits ($\overline{T}$, $\underline{T}$, $\overline{\dot{T}}$, $\underline{\dot{T}}$, $\overline{\Gamma}$, $\underline{\Gamma}$, $\overline{\dot{\Gamma}}$, $\underline{\dot{\Gamma}}$) are given by equations (51) - (54) in section 3.5.

4.4. CA Approach 2 - derivation of LTV effector mapping

Given the nonlinear effector mapping given in equation (5), by means of a time discretisation we can approximate the problem to a sequence of linear control allocation problems. The proposed solution is given by the following steps:

1. Sample the signals $\boldsymbol{\tau}(t)$, $\mathbf{x}(t)$ $\mathbf{u}(t)$, $\boldsymbol{\tau}_c(t)$ with a sample time of Δt so that $\boldsymbol{\tau}_k = \boldsymbol{\tau}(k\Delta t)$, $\mathbf{x}_k = \mathbf{x}(k\Delta t)$, $\mathbf{u}_k = \mathbf{u}(k\Delta t)$, $\boldsymbol{\tau}_{ck} = \boldsymbol{\tau}_c(k\Delta t)$ for $k = 0, 1, 2, \ldots$, etc.
2. For each sample point, k, let $\Delta\boldsymbol{\tau}(k\Delta t) = \boldsymbol{\tau}(k\Delta t + \Delta t) - \boldsymbol{\tau}(k\Delta t)$ etc.
3. Given $\boldsymbol{\tau}(k\Delta t) = \mathbf{g}_e(\mathbf{x}(k\Delta t), \mathbf{u}(k\Delta t))$, and dropping the notational dependence on $k\Delta t$, we get the Taylor's expansion

$$\mathbf{g}_e(\mathbf{x} + \Delta\mathbf{x}, \mathbf{u} + \Delta\mathbf{u}) = \mathbf{g}_e(\mathbf{x}, \mathbf{u}) + \frac{\partial \mathbf{g}_e}{\partial \mathbf{x}}\Delta\mathbf{x} + \frac{\partial \mathbf{g}_e}{\partial \mathbf{u}}\Delta\mathbf{u} + \text{ higher order terms} \tag{62}$$

Ignoring second and higher order terms gives

$$\Delta\boldsymbol{\tau} = \mathbf{G}_x\Delta\mathbf{x} + \mathbf{G}_u\Delta\mathbf{u} \tag{63}$$

where

$$\mathbf{G}_x(k\Delta t) = \left[\frac{\partial \mathbf{g}_e(\mathbf{x}, \mathbf{u})}{\partial \mathbf{x}}\right]_{\substack{\mathbf{x}=\mathbf{x}(k\Delta t) \\ \mathbf{u}=\mathbf{u}(k\Delta t)}}$$

$$\mathbf{G}_u(k\Delta t) = \left[\frac{\partial \mathbf{g}_e(\mathbf{x}, \mathbf{u})}{\partial \mathbf{u}}\right]_{\substack{\mathbf{x}=\mathbf{x}(k\Delta t) \\ \mathbf{u}=\mathbf{u}(k\Delta t)}} \tag{64}$$

4. We now have a linear control allocation equation

$$\mathbf{G}_u\Delta\mathbf{u} = \Delta\boldsymbol{\tau} - \mathbf{G}_x\Delta\mathbf{x} \tag{65}$$

which, along with magnitude and slew rate constraints can be solved at each time step k using classical control allocation methods.

$$\mathbf{G}_u = \left[\frac{\partial \mathbf{g}_e(\mathbf{x}, \mathbf{u})}{\partial \mathbf{u}}\right]_{\mathbf{u}=\mathbf{u}(k\Delta t)} \tag{66}$$

$$= \begin{bmatrix} \cos\Gamma_f & \cos\Gamma_a & -T_f \sin\Gamma_f & -T_a \sin\Gamma_a \\ -\sin\Gamma_f & -\sin\Gamma_a & -T_f \cos\Gamma_f & -T_a \cos\Gamma_a \\ -\ell_f \sin\Gamma_f & \ell_a \sin\Gamma_a & -\ell_f T_f \cos\Gamma_f & \ell_a T_a \cos\Gamma_a \end{bmatrix}. \tag{67}$$

Note that for this system, $\mathbf{G}_x = 0$ since the aerodynamics and their couplings with propulsive forces are not considered, unlike traditional aircraft control surfaces (e.g. rudder, aileron, elevators etc.) where the control effectiveness depends not only on the control deflections but also on the states (e.g. airspeed V, AoA or theta for wing level, level flight etc.).

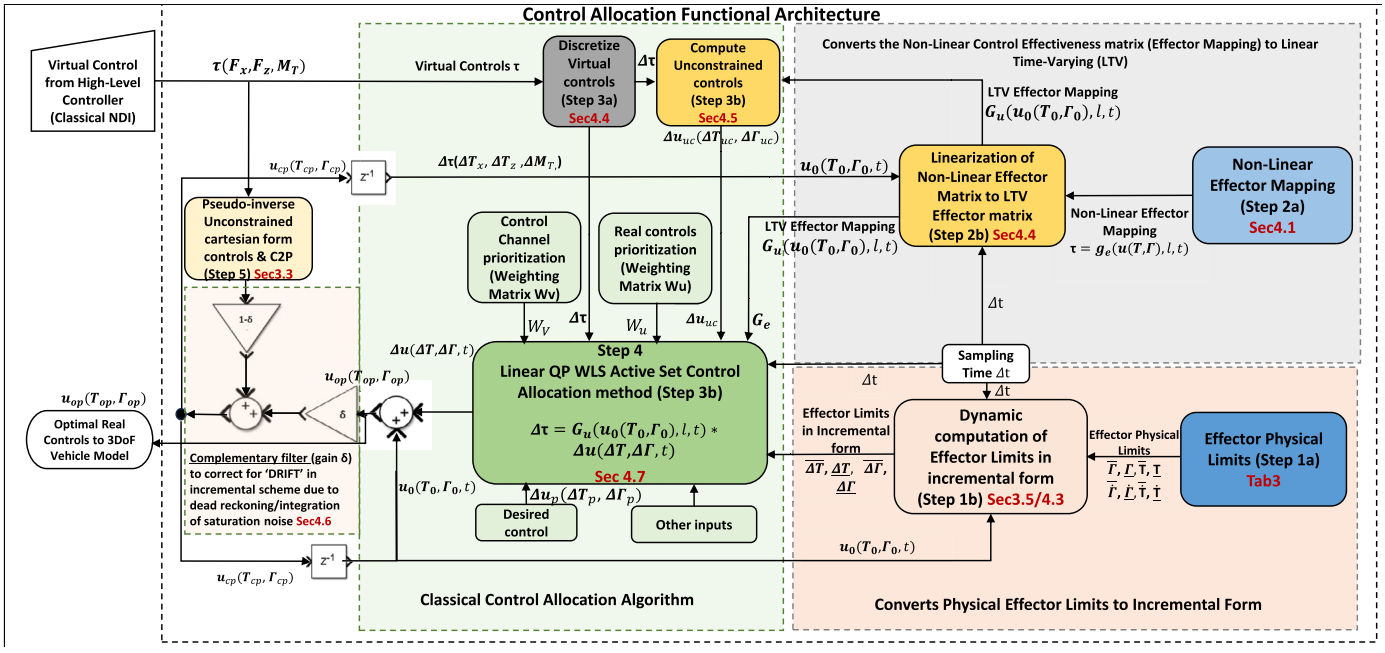

Fig. 11. CA Approach 2 Functional Architecture.

4.5. CA Approach 2 - computation of unconstrained real controls

The unconstrained real control is given by:

$$\mathbf{u}_{uc} = \mathbf{G}_{\mathbf{u}}^{+}(\mathbf{x},t)\boldsymbol{\tau}_c \tag{68}$$

where:

$$\mathbf{G}_{\mathbf{u}}^{+}(\mathbf{x},t) = \mathbf{G}_u(\mathbf{x},t)^T(\mathbf{G}_u(\mathbf{x},t)\mathbf{G}_u(\mathbf{x},t)^T)^{-1} \tag{69}$$

4.6. CA Approach 2 - correction of drift

The complementary filter is shown in step 5 of Fig. 11. The drift correction update is done using the unconstrained controls of CA Approach 1 in equations (25) to (29) and then transformed from cartesian form to compatible polar form using equation (30) with a gain set to 0.95 resulting in only 5% of the update source and 95% of the incremental scheme constituting the final control which is subsequently constrained by the incremental actuator limits in the classical CA algorithm (Active Set).

4.7. CA Approach 2 - prioritised incremental linear control allocation

To solve the CA problem in equation (20), the absolute values of virtual and real controls were changed to incremental (Δ) value. Following the active set described in [13], the problem is first formulated in weighted least squares form below:

$$\Delta\mathbf{u}_{op} = \arg\min_{\underline{\Delta\mathbf{u}}\le\Delta\mathbf{u}\le\overline{\Delta\mathbf{u}}} \left\|\mathbf{W}_u(\Delta\mathbf{u}-\Delta\mathbf{u}_p)\right\|^2 + \gamma\left\|\mathbf{W}_v(\mathbf{B}\Delta\mathbf{u}-\Delta\boldsymbol{\tau})\right\|^2 \tag{70}$$

The cost function is incorporated in ***Algorithm 3***.

5. Control Allocation Approach 3

A final contribution of this work is CA 3 which is similar to CA 2 except an extra step which transforms the virtual controls from cartesian to polar before differentiation and linearisation resulting in a different and more complicated LTV Effector mapping (Jacobian of $\boldsymbol{\tau}$ with respect to $\mathbf{u}$). The other aspects (incremental actuator constraints and Active Set WLS Prioritised constrained CA) are the same as can be seen from the functional architectures in Figs. 8 and 11. Also, the linearisation is analytical which is more accurate than numeric linearisation for the case

Algorithm 3 - Active set algorithm for Weighted LS [13].

1. Let $\mathbf{u}^0$ and $\mathbf{W}$ be the optimal solution and working set respectively from the previous sampling instant.
2. Rewrite the cost function as:

$$\left\|\mathbf{W}_u(\Delta\mathbf{u}-\Delta\mathbf{u}_p)\right\|^2 + \gamma\left\|\mathbf{W}_v(\mathbf{G}_e\Delta\mathbf{u}-\Delta\boldsymbol{\tau})\right\|^2 = \left\|\begin{pmatrix}\gamma\mathbf{W}_v\mathbf{G}_e\\ \mathbf{W}_u\end{pmatrix}\Delta\mathbf{u} - \begin{pmatrix}\gamma\mathbf{W}_v\Delta\boldsymbol{\tau}\\ \mathbf{W}_u\Delta\mathbf{u}_p\end{pmatrix}\right\|$$

3. and solve

$$\Delta\mathbf{u}_{op} = \arg\min_{\underline{\Delta\mathbf{u}}\le\Delta\mathbf{u}\le\overline{\Delta\mathbf{u}}} \left\|\mathbf{A}_{as}\Delta\mathbf{u}-\mathbf{q}\right\|$$

using ***Algorithm 4*** where $\mathbf{A}_{as}$ and $\mathbf{q}$ are as defined in equations (56) and (57).

of Approach 2. The transformation of the virtual control to same polar form as the real controls and actuator limits has the advantage that the resulting effector mapping though more complex, is more linear in the real controls and actuator limits.

It offers a real-time analytical optimal control allocation (i.e., doesn't utilize optimization software and linearized effector model – control effectiveness matrix) which considers both actuator saturation and rate limits using active set Prioritised linear QP Weighted Least squares (WLS) formulation as the linear control allocation algorithm. The control allocation also relies on the feedback control of the system to account for uncertainty in the effector-control mappings.

5.1. CA Approach 3 effector model formulation

The 3DoF aircraft model showing the effector model is the same as in Fig. 10 and the effector mapping same as in equations (59) - (61).

5.2. CA Approach 3 functional architecture

The control allocation architecture is shown in Fig. 12 and consist of five steps:

- *Step 1 - Conversion of the actuator constraints from absolute to incremental limits*

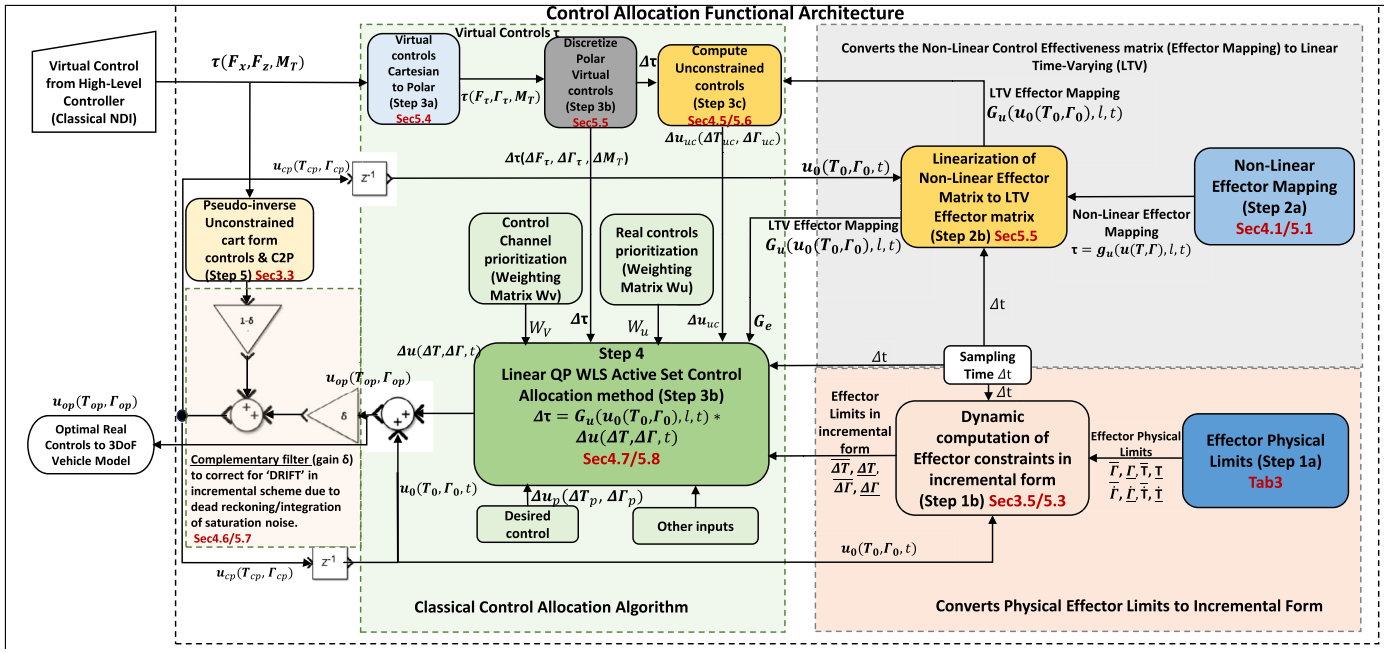

Fig. 12. CA Approach 3 Functional Architecture.

Algorithm 4 - Active Set Algorithm [13].

1. Let $\Delta\mathbf{u}^0$ be a feasible starting point. A point is feasible if it satisfies both the control constraint ($\mathbf{G}_e\Delta\mathbf{u} = \Delta\boldsymbol{\tau}$) and actuator constraints ($\underline{\Delta\mathbf{u}} \le \Delta\mathbf{u} \le \overline{\Delta\mathbf{u}}$).
2. Let the working set $\mathbf{W}$ contain (a subset of) the active inequality constraints at u^0
3. **for** $k = 0, 1, 2..., N-1$ **do**
4. Given $\Delta\mathbf{u}^k$ the value of $\Delta\mathbf{u}$ at the k^{th} step, find the optimal perturbation $\mathbf{p}$, considering the constraints in the working set as equality constraints and disregarding the remaining inequality constraints. Solve

$$\min_{\mathbf{p}} \left\|\mathbf{A}_{as}(\Delta\mathbf{u}_k + \mathbf{p}) - \mathbf{G}_e\right\|$$
$$\mathbf{G}_e\mathbf{p} = 0 \tag{71}$$
$$\mathbf{p}_i = 0, i \in \mathbf{W}$$

where $\mathbf{A}_{as}$ and $\mathbf{q}$ are as defined in equations (56) and (57)

5. **if** $\Delta\mathbf{u}^k + \mathbf{p}$ is feasible **then**
6. Set $\Delta\mathbf{u}^{k+1} = \Delta\mathbf{u}^k + \mathbf{q}$ and compute the Lagrange multipliers, $\begin{pmatrix}\boldsymbol{\mu}\\ \lambda\end{pmatrix}$, where $\boldsymbol{\mu}$ and λ are associated with the control constraint ($\mathbf{B}\Delta\mathbf{u} = \Delta\boldsymbol{\tau}$) and actuator constraints ($\underline{\Delta\mathbf{u}} \le \Delta\mathbf{u} \le \overline{\Delta\mathbf{u}}$) respectively
7. **if** all elements of $\lambda \ge 0$ **then**
8. $\Delta\mathbf{u}_{op} = \Delta\mathbf{u}^{k+1}$ is the optimal solution to equation (71).
9. **else**
10. Remove the constraint associated with the most negative λ from the working set
11. **else**

Determine the maximal step length α such that α such that $\Delta\mathbf{u}^{k+1} = \Delta\mathbf{u}^k + \alpha\mathbf{p}$ is feasible. Add the primary bounding constraint to the working set.

12. **end**

- *Step 2 - Linearization of the Non-Linear Effector mapping to Linear-Time-Varying Effector Mapping*
- *Step 3 - Conversion of virtual controls from cartesian to polar, discretisation of virtual controls and computation of unconstrained real controls*
- *Step 4 - Application of classical constrained linear control allocation technique*
- *Step 5 - Correction of drift using complementary filter*

5.3. Approach 3 - incremental constraints formulation

Again, the incremental actuator limits are given by equations (51) - (54) in section 3.5.

5.4. Approach 3 - conversion of the virtual controls from cartesian to polar

Following on from the effector model formulation in section 5.1, the relationship between the virtual controls in the polar body axes and the real controls is then:

$$F_\tau \sin\Gamma_\tau = T_f \sin\Gamma_f + T_a \sin\Gamma_a, \tag{72}$$
$$F_\tau \cos\Gamma_\tau = T_f \cos\Gamma_f + T_a \cos\Gamma_a, \tag{73}$$

giving

$$F_\tau = \sqrt{(T_a\cos\Gamma_a + T_f\cos\Gamma_f)^2 + (T_a\sin\Gamma_a + T_f\sin\Gamma_f)^2}, \tag{74}$$
$$\Gamma_\tau = \operatorname{atan2}(T_a\sin\Gamma_a + T_f\sin\Gamma_f, T_a\cos\Gamma_a + T_f\cos\Gamma_f), \tag{75}$$
$$M_T = \ell_f T_f \sin\Gamma_f - \ell_a T_a \sin\Gamma_a. \tag{76}$$

5.5. CA Approach 3 - derivation of LTV effector mapping

In this Control Allocation Approach 3, we propose a simple mechanism to transform such non-linear problems to linear problems. This is done by analytical linearization by taking small perturbations to ensure the linearization step is accurate. Classical control allocation can then be applied and the constraints satisfied. The resulting point in the effector space is tracked and the process repeated at each time-step. Again the scheme relies on the feedback control of the system to account for uncertainty in the linearization and effector-control mappings.

Linearizing equations (74) - (76) with small perturbations we get

$$\begin{bmatrix}\Delta F_\tau\\ \Delta\Gamma_\tau\\ \Delta M_T\end{bmatrix} = \begin{bmatrix}(T_f + T_a\cos\Gamma_{\tau 2})d & (T_a + T_f\cos\Gamma_{\tau 2})d & T_aT_f\sin\Gamma_{\tau 2}d & -T_aT_f\sin\Gamma_{\tau 2}d\\ -T_a\sin\Gamma_{\tau 2}d^2 & T_f\sin\Gamma_{\tau 2}d^2 & T_f(T_f + T_a\cos\Gamma_{\tau 2})d^2 & T_a(T_a + T_f\cos\Gamma_{\tau 2})d^2\\ \ell_f\sin\Gamma_f & -\ell_a\sin\Gamma_a & \ell_f T_f\cos\Gamma_f & -\ell_a T_a\cos\Gamma_a\end{bmatrix}\begin{bmatrix}\Delta T_f\\ \Delta T_a\\ \Delta\Gamma_a^f\\ \Delta\Gamma_a^f\end{bmatrix} \tag{77}$$

where

$$d = \frac{1}{(T_a^2 + 2T_aT_f\cos\bar{\Gamma} + T_f^2)^{1/2}} \tag{78}$$

and $\bar{\Gamma} = \Gamma_a - \Gamma_f$. We now have a linear control allocation equation

$$\Delta\boldsymbol{\tau} = \mathbf{G}_u\Delta\mathbf{u} \tag{79}$$

which, along with magnitude and slew rate constraints can be solved at each time step k using classical control allocation methods. The gradient matrix $\mathbf{G}_u$ is given by:

$$\mathbf{G}_u = \left[\frac{\partial\mathbf{g}_e(\mathbf{u})}{\partial\mathbf{u}}\right]_{\mathbf{u}=\mathbf{u}(kT)} \tag{80}$$

$$= \begin{bmatrix} (T_f + T_a\cos\Gamma_{\tau 2})d & (T_a + T_f\cos\Gamma_{\tau 2})d & T_aT_f\sin\Gamma_{\tau 2}d & -T_aT_f\sin\Gamma_{\tau 2}d \\ -T_a\sin\Gamma_{\tau 2}d^2 & T_f\sin\Gamma_{\tau 2}d^2 & T_f(T_f + T_a\cos\Gamma_{\tau 2})d^2 & T_a(T_a + T_f\cos\Gamma_{\tau 2})d^2 \\ \ell_f\sin\Gamma_f & -\ell_a\sin\Gamma_a & \ell_fT_f\cos\Gamma_f & -\ell_aT_a\cos\Gamma_a \end{bmatrix} \tag{81}$$

5.6. CA Approach 3 - computation of unconstrained real controls

The unconstrained real control is as given in equation (68) and (69) for CA Approach 2.

5.7. CA Approach 3 - correction of drift

The drift correction update is shown in step 5 of Fig. 12 and is same as that in CA Approach 2 in section 4.6.

5.8. Approach 3 - prioritised incremental linear control allocation

Refer to section 4.7 for Algorithms 3 and 4 presented in CA Approach 2.

6. Simulations results and discussions

The vehicle model and NDI controller are coded in Simulink® and MATLAB® simulation software. All the simulations are conducted in MATLAB® Simulink® with Software version R2021b on a personal computer of Intel Core i9-8950H 2.90 GHz CPU and 32 GB RAM. The MATLAB® simulation was run at a fixed step sample time of 10 ms (100 Hz). The constants (outer-loop controller parameters, pilot command limits and control limits) used for the model are given in Table 2 with an assumption of noise-free measurements. The Actuator Constraints and Dynamics are presented in Table 3. Also, the inputs constants into the prioritised constrained linear optimisation Active Set algorithm are listed in Table 4, where:

$$\mathbf{W}_v = \begin{bmatrix} 1 & 0 & 0 \\ 0 & 2 & 0 \\ 0 & 0 & 10 \end{bmatrix} \tag{82}$$

$$\mathbf{W}_u = \mathbf{I}_4 \tag{83}$$

As discussed in section 1, the values of $\mathbf{W}_v$ in equation (82) are chosen so that pitch rate q has the highest priority, followed by body z-axis velocity w before body x-axis velocity u. The rotational channel (pitch rate q) is prioritised over translational channels (heave w and surge u) to maintain stable and safe flight during limited control authority due to actuator saturation (rate or position) because rotational channels tracking is more critical in ensuring stable flight compared to translation channel tracking for VTOLs. Similarly, for the translational channels, the body z-axis velocity w tracking error minimisation is more critical in maintaining stable flight than body x-axis velocity u error tracking. Furthermore, during limited control authority where all remaining control authority allocated to the pitch rate is sufficient, this could potentially only result in degraded performance (poor u and w tracking) but safe and stable flight would be maintained since rotational channels have the tendency to cause instability more than translational channels.

Table 2
Simulink simulation coefficients.

Quantity or Parameters	Value
Total mass, m	1.0 kg
Gravitational constant, g	9.81 m s^{-2}
Moment of inertia in the pitch axis, I_{yy}	2 kg m s^2
Inner loop NDI u tracking loop P gain, K_{up}	1.5 N m^{-1} s
Inner loop NDI w tracking loop P gain, K_{wp}	1.5 N m^{-1} s
Inner loop NDI q loop P gain, K_{qp}	1.5 N m rad^{-1} s
Outer loop altitude control P gain, K_{hp}	1.5 N m rad^{-1}
Outer loop altitude control integral gain, K_{hi}	0.2 N m rad^{-1}
Outer loop attitude control P gain, $K_{\theta p}$	1.5 N m rad^{-1}
Outer loop position hold loop P gain, K_{xp}	1 N m^{-1}
Outer Loop lateral position hold loop integral gain, K_{xi}	0.005 N m^{-1}
Canard Moment Arm (ℓ_c)	1 m
Main Wing Moment Arm (ℓ_w)	1 m
Total Airspeed Pilot command upper limit on r_u	8g m s^{-1}
Total AirSpeed Pilot command lower limit on r_u	−5 m s^{-1}
Total AirSpeed Pilot command rate limit on r_u	±4 m s^{-2}
Flight Path Angle Pilot command upper limit $\bar{\gamma}$	4° s^{-1}
Flight Path Angle Pilot command lower limit $\underline{\gamma}$	−2° s^{-1}
Pitch Attitude Pilot command limit on r_θ	±10°
Pilot command rate limits on pitch angle rate $\dot{r}_q$	±0.4° s^{-1}
Altitude Pilot command upper limit on r_h	3000 m
Altitude Pilot command lower limit on r_h	−1000 m
Altitude Pilot command upper rate limit on r_h	5 m/s
Altitude Pilot command lower rate limit on r_h	−4 m/s

Table 3
Actuator Physical Limits and Dynamics.

Actuator control input	ω_n	ζ	Minimum	Maximum	Rate Limit
Thrust for all EDFs	25 rad/s	1	0 N	5.7 N	±4 N/s
Γ for canard EDFs	20 rad/s	1	-30°	100°	±30°/s
Γ for wing EDFs	20 rad/s	1	0°	100°	±30°/s

Table 4
Active Set CA Algorithm Input Constants.

Input Constant name	Symbol	Type	Order	Value
Linear Effectiveness Matrix	$\mathbf{B}_u$ or $\mathbf{G}_u$	$Matrix$	$\mathbb{R}^{3\times4}$	See Eqn. (66)
Virtual control weighting matrix	$\mathbf{W}_v$	$Matrix$	$\mathbb{R}^{3\times3}$	See Eqn. (82)
Control weighting matrix	$\mathbf{W}_u$	$Matrix$	$\mathbb{R}^{4\times4}$	See Eqn. (83)
Primary objective weighting factor	γ	$scalar$	$\mathbb{R}$	10^6
Maximum number of iterations	i_{max}	$scalar$	$\mathbb{R}$	10
WLS Algorithm Simulation Period	Δt	$scalar$	$\mathbb{R}$	10^{-2}

Although the effector configuration used throughout this study is over-actuated (four real control variables to control only three degrees of freedom), there is however no redundancy because both the front and rear EDFs are required to maintain stable flight. Hence $\mathbf{W}_u$ is set to the identity matrix so no penalties are applied on any of the real controls.

Furthermore, considering the real time implementation, the maximum CA software iterations i_{max} is set to 10 to ensure that the CA algorithm is constrained to find the optimal solution within a short time. Moreover, the CA algorithm does not cause discontinuities/sudden jumps in the actuator positions since it always finds an optimal solution even while considering both actuator slew rate and position limits which is crucial for the real time implementation.

Furthermore, the γ is set to a high value of 10^6 to ensure that the primary objective of control error minimisation with weighting matrix W_v is properly distinguished from secondary objective of control effort minimisation with weighting matrix of W_u.

Finally, the working set $\mathbf{W}$ of the Active Set CA algorithm is vector whose elements indicates which of the effectors are saturated or not and is explained as follows: $\mathbf{W} = \begin{bmatrix} W1 & W2 & W3 & W4 \end{bmatrix}^T$ whether the control allocation is active or not, explained as follows:

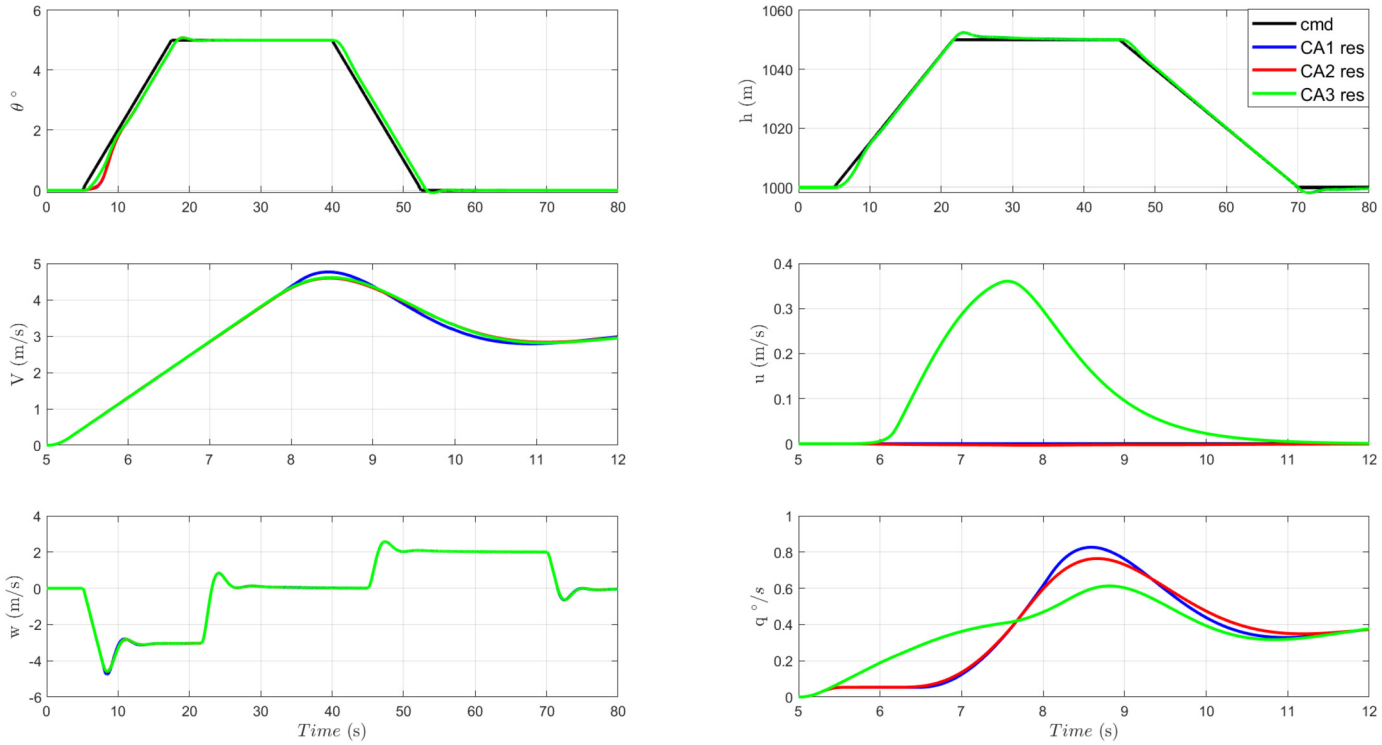

Fig. 13. VTO/VL with pitch control - States. (For interpretation of the colours in the figure(s), the reader is referred to the web version of this article.)

- $W*=0$ means no actuator saturation, $W*=-1$ means actuator saturation at lower limit, $W*=1$ means actuator saturation at upper limit
- $W1$ means fore EDF thrust body x-axis component for CA1, means fore actuator EDFs thrust/rpm for CA2 and CA3
- $W2$ means aft EDF thrust body x-axis component for CA1, means aft actuator EDFs thrust/rpm for CA2 and CA3
- $W3$ means fore EDF thrust body z-axis component for CA1, means fore actuator EDFs tilt angle for CA2 and CA3
- $W4$ means fore EDF thrust body z-axis component for CA1, means aft actuator EDFs tilt angle for CA2 and CA3

In order to test the effectiveness of the control allocation approaches, two selected critical aircraft control manoeuvres are investigated considering the longitudinal motion of the planar VTOL. These aircraft control manoeuvres (ACM) are not typical realistic flight test manoeuvres (FTM) but chosen to test the ability of the CA to allocate remaining control authority to higher priority and critical control channels in order to maintain operational safety and stability during certain flight conditions while there is limited control authority due to actuator saturation. The actuator (thrust and tilting mechanism) limits (position and rates) are intentionally set tighter than in reality so that they are violated thereby activating the Active Set linear CA algorithm as some point. The first ACM (ACM 1) aims to test how the control allocation responds when maximum actuator thrust limits are reached during a vertical take-off (VTO)/Vertical Landing (VL) scenarios with pitch control, and Hover to high forward speed. The second ACM (ACM 2) aims to test how the control allocation responds when maximum actuator tilt angle limits is reached during a Reverse manoeuvre with pitch control. Another way of testing the CA responds when maximum actuator tilt angle limits are reached is by performing a deceleration from high forward speed to hover. One way of testing the CA response to minimum actuator tilt angle limits violation will be performing a transition from hover to cruise (forward transition) on a full aerodynamic aircraft when the wing tilt angles can tilt close to its lower limit. The two selected ACMs are detailed below.

6.1. ACM 1 - VTO/VL with pitch control and limited control authority

The manoeuvre starts at hover altitude of $h = 1000$ m. At time $t = 5$ s, a VTO altitude of 1050 m at constant climb rate of 4 m/s is commanded for 12.5 s. Simultaneously, (at same $t = 5$ s), a pitch attitude θ of 5° at a constant rate of ± 0.01 rad s^{-1} was commanded. At time $t = 45$ s, A VL hover altitude of 1000 m was commanded at constant descend rate of 2 m/s for 25 s. Simultaneously, (at same $t = 45$ s), a pitch attitude (θ) of 0° at a constant rate of ± 0.01 rad s^{-1} is commanded. The commanded and actual states, commanded and actual effector positions, virtual controls, control authority (actuator limitation) status, state tracking error as well as virtual control tracking errors are shown for all three control allocation approaches from Figs. 13 - 16.

Analysis of ACM 1 results During the initial phase of the VTO, as can be seen from Fig. 15, the high-level controller outputs violated the maximum thrust limit ($W1$ and $W2$ for CA2 and CA3) and tilt angle rates ($W3$ and $W4$ for CA2 and CA3) limits between $5s$ and $7s$ resulting the CAs being active (see Fig. 16) imposing actuator constraints limitations on the CA output which prevent violation of the physical actuator constraints. While the CAs were active due to actuator thrust saturation, the CAs allocates the limited control authority to the highest priority rotational channel pitch rate/pitching moment (see equation (82) and discussion in section 2.3.2) resulting in lower q error compared to u and w as can be seen from Figs. 13 and 14. In terms of comparison of the three CA schemes, they perform similarly except that CA2 and CA3 (green) additionally imposed a minimum thrust rate limitation at time $22s$ at the end of the VTO command (Fig. 16). Also, CA1 seems to converge faster (fewer number of CA software iterations CA_{iter}) than CA2 and CA3 for the same manoeuvre (Fig. 16). The performances for all three CA schemes are also investigated considering the real time implementation. According to Fig. 16, the maximum CA software iterations CA_{iter} are below 10 when the CA is active. Therefore, the CA algorithm finds the optimal solution quickly. Moreover, the CA algorithm does not cause discontinuities/sudden jumps in the actuator positions which is crucial for the real time implementation because it was able to find

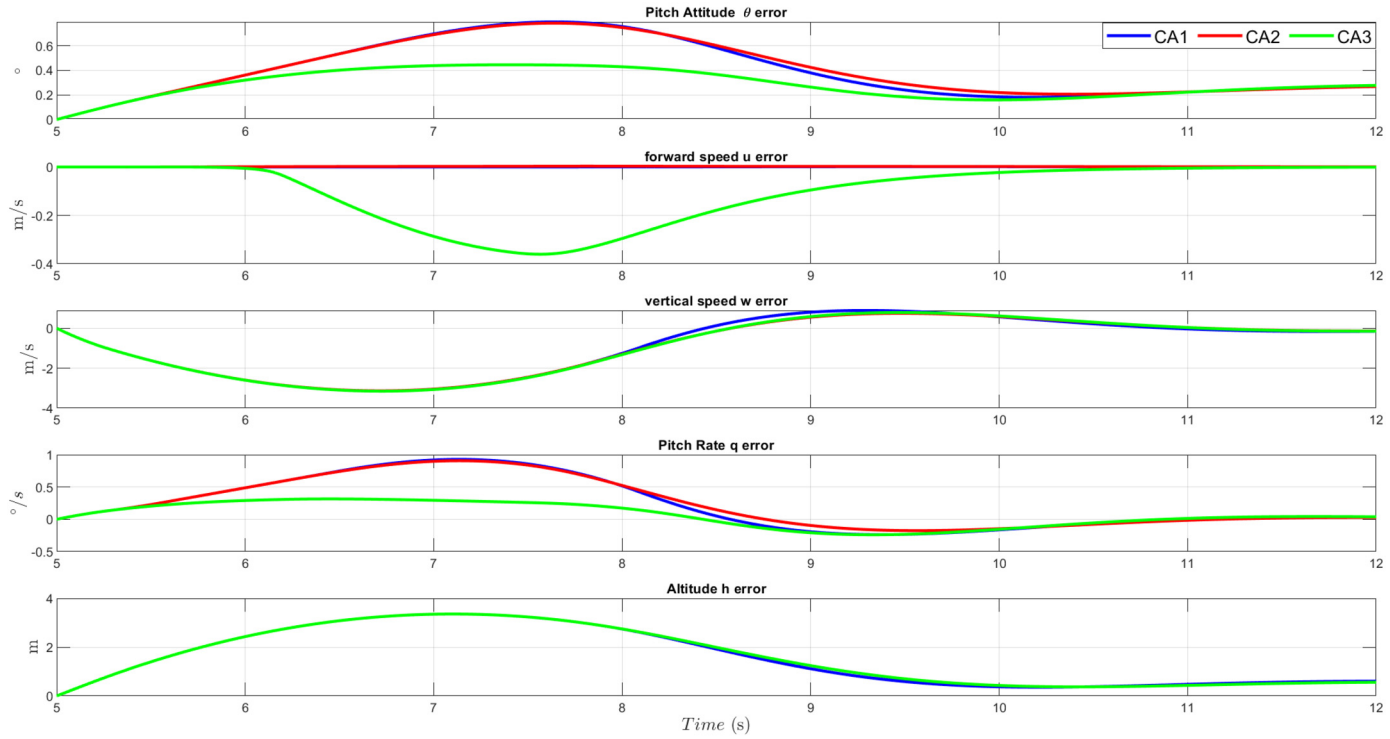

Fig. 14. VTO/VL with pitch control - States Error.

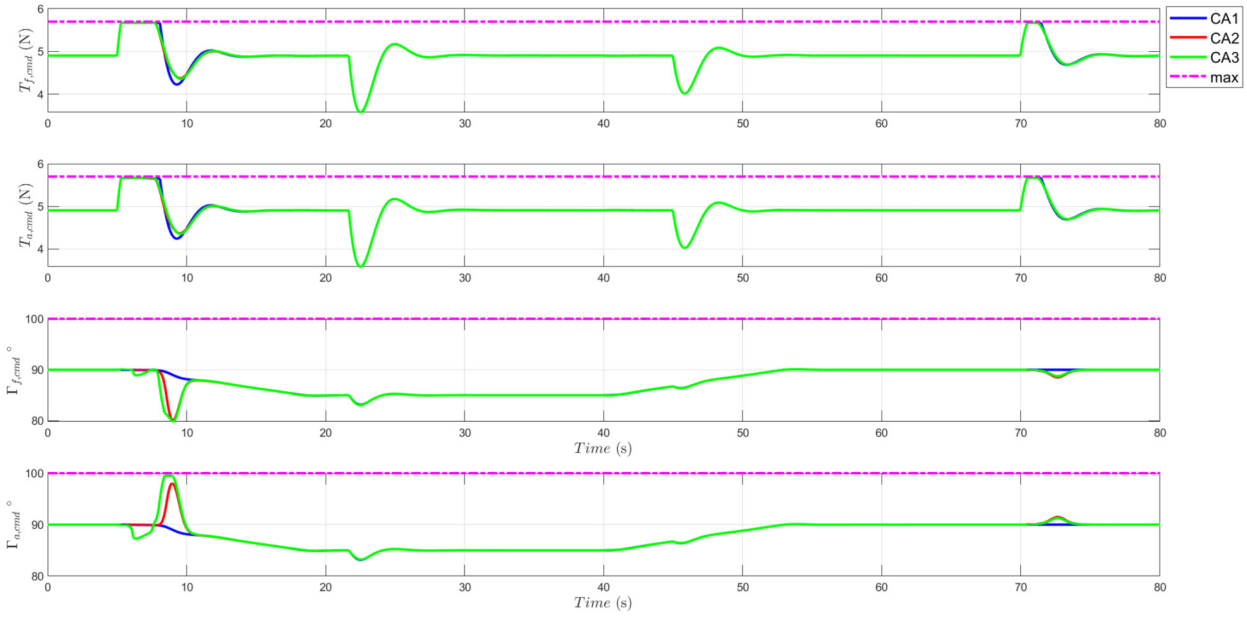

Fig. 15. VTO/VL with pitch control - Effector commands.

optimal solution subjected to both the actuator slew rate and position limits. In the absence of any control authority limitation, the control allocation correctly allocates the overall control demand from the high-level controller to the individual control effectors/actuators resulting in accurate tracking of pilot commands.

6.2. ACM 2 - reverse backward and pitch control with limited control authority

The manoeuvre start at hover altitude of h =1000 m. At time $t = 5$ s, a reverse at -5 m/s was commanded. Simultaneously, (at same $t = 5$ s), a pitch attitude θ of 5° at a constant rate of ± 0.01 rad s^{-1} was commanded. At time $t = 20$ s, the pitch attitude θ of 5° was then cancelled (commanded to θ of 0°) at a constant rate of ± 0.01 rad s^{-1}. The commanded and actual states, commanded and actual effector positions, virtual controls, control authority (actuator limitation) status, state tracking error as well as virtual control tracking errors are shown for all three control allocation approaches in Figs. 17 - 20.

Analysis of ACM 2 results During the initial phase of the reverse speed manoeuvre, as can be seen from Fig. 19, the high-level controller outputs violated the tilt angle rates ($W3$ and $W4$) limits for CA2 and CA3 (and body x-axis horizontal thrust $u_{x,f}$ and $u_{x,a}$ lower limit in CA1) be-

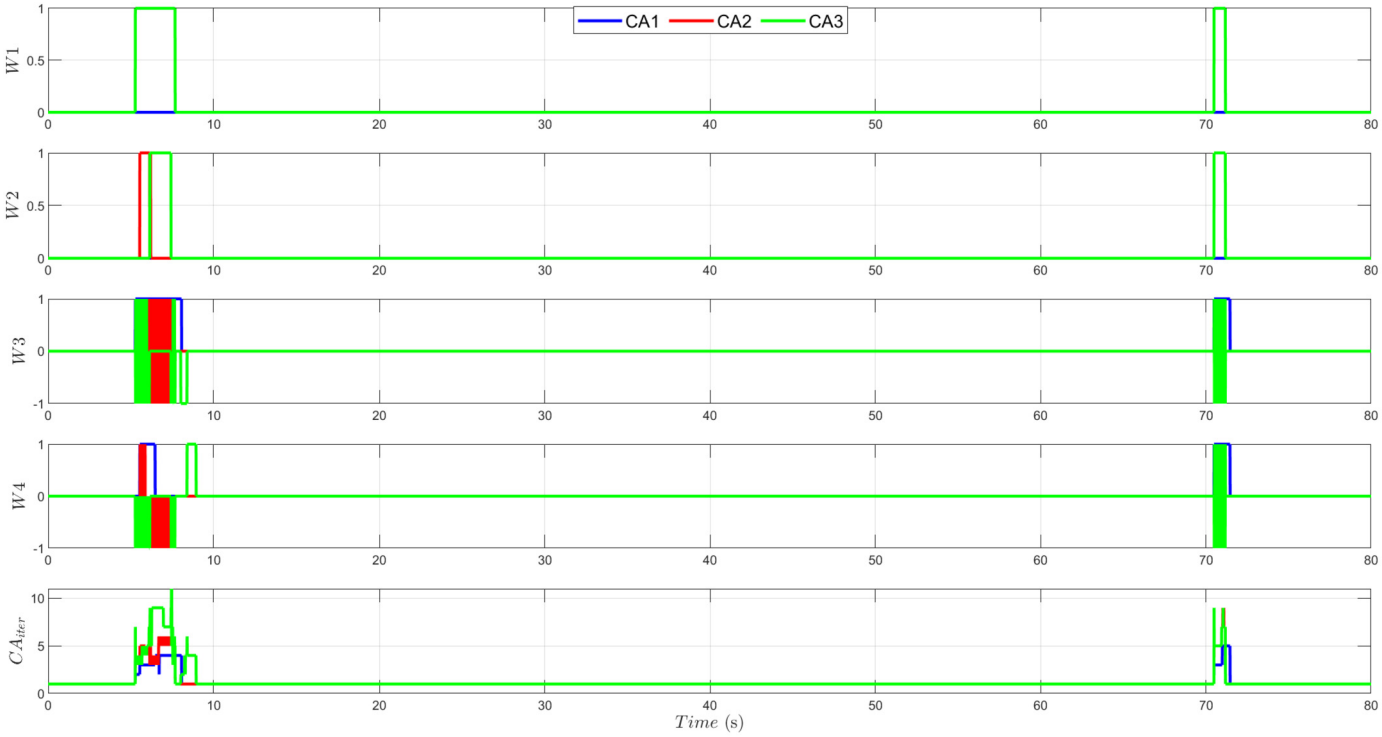

Fig. 16. VTO/VL with pitch control - Control limitation status.

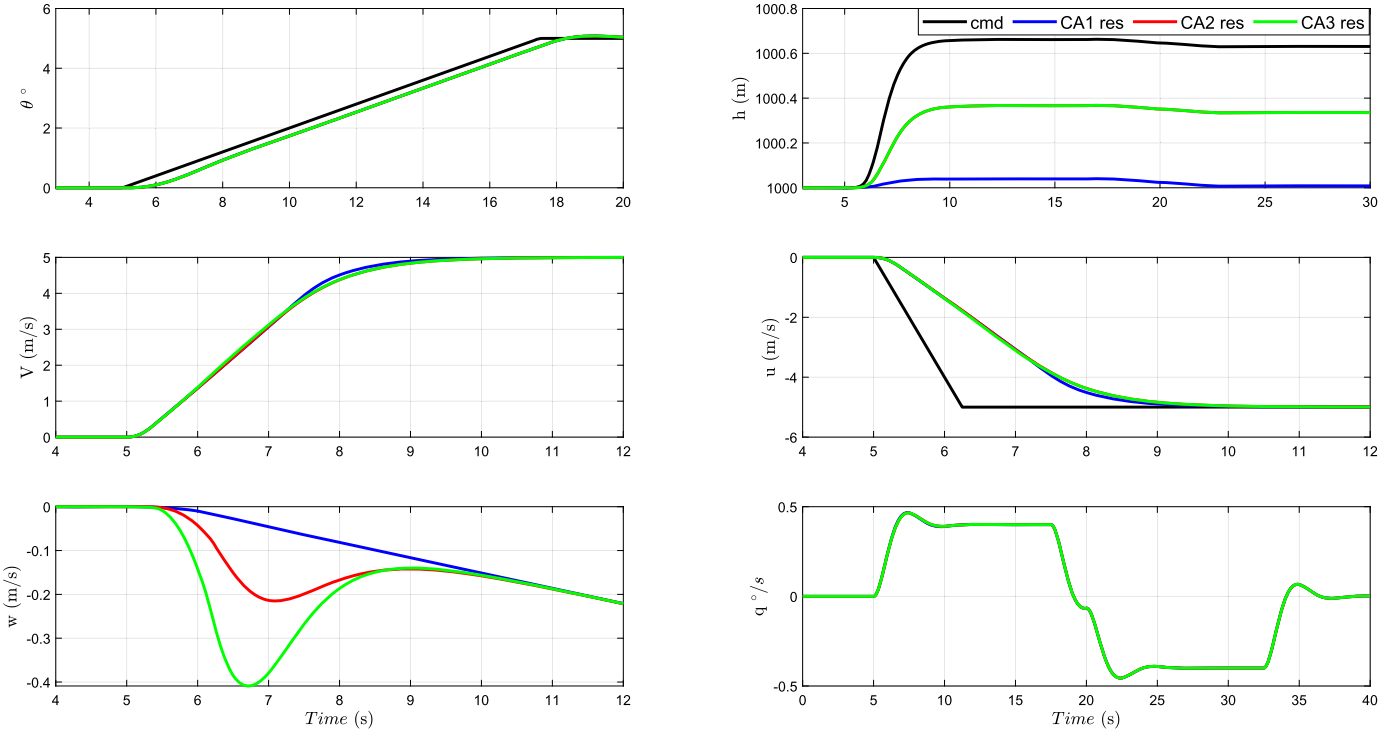

Fig. 17. Reverse backward and pitch control - States.

tween 5 s and 7.5 s resulting the CAs being active (see Fig. 20) imposing actuator constraints limitations on the CA output which prevent violation of the physical actuator constraints. Again, while the CAs were active due to actuator tilting mechanism saturation, the CAs allocates the limited control authority to the highest priority rotational channel pitch rate/pitching moment (see equation (82) and discussion in section 2.3.2) resulting in lower q error compared to u and w as can be seen from Figs. 17 and 18. Also, between 5 s and 7.5 s there was a 25% increase in both rotor thrust for both CA2 and CA3 compared to only 8% increase for CA1. Again CA1 seems to converge faster (lower number of CA software iterations CA_{iter}) than CA2 and CA3 for same manoeuvre (Fig. 20). The performances for all three CA schemes are also investigated considering the real time implementation. According to Fig. 20, the maximum CA software iterations CA_{iter} are below 13 when the CA

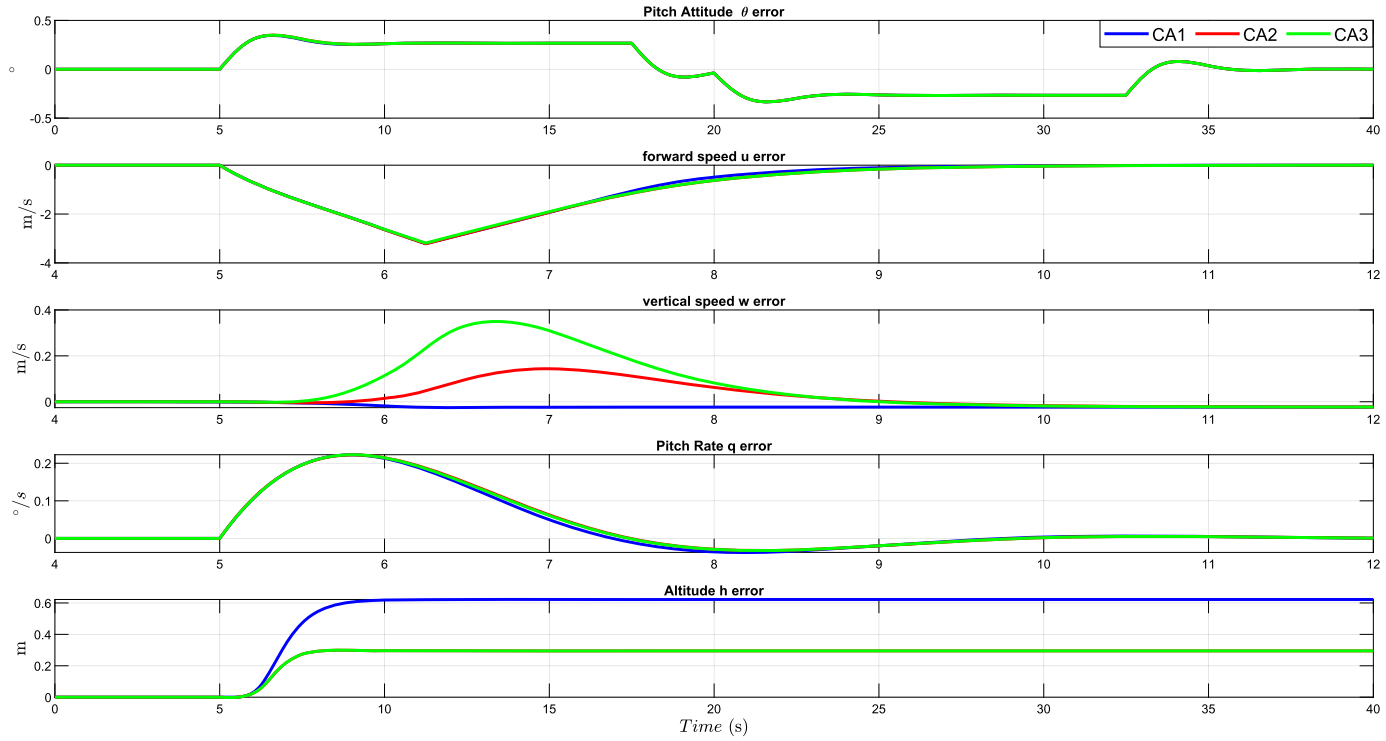

Fig. 18. Reverse backward and pitch control - States Error.

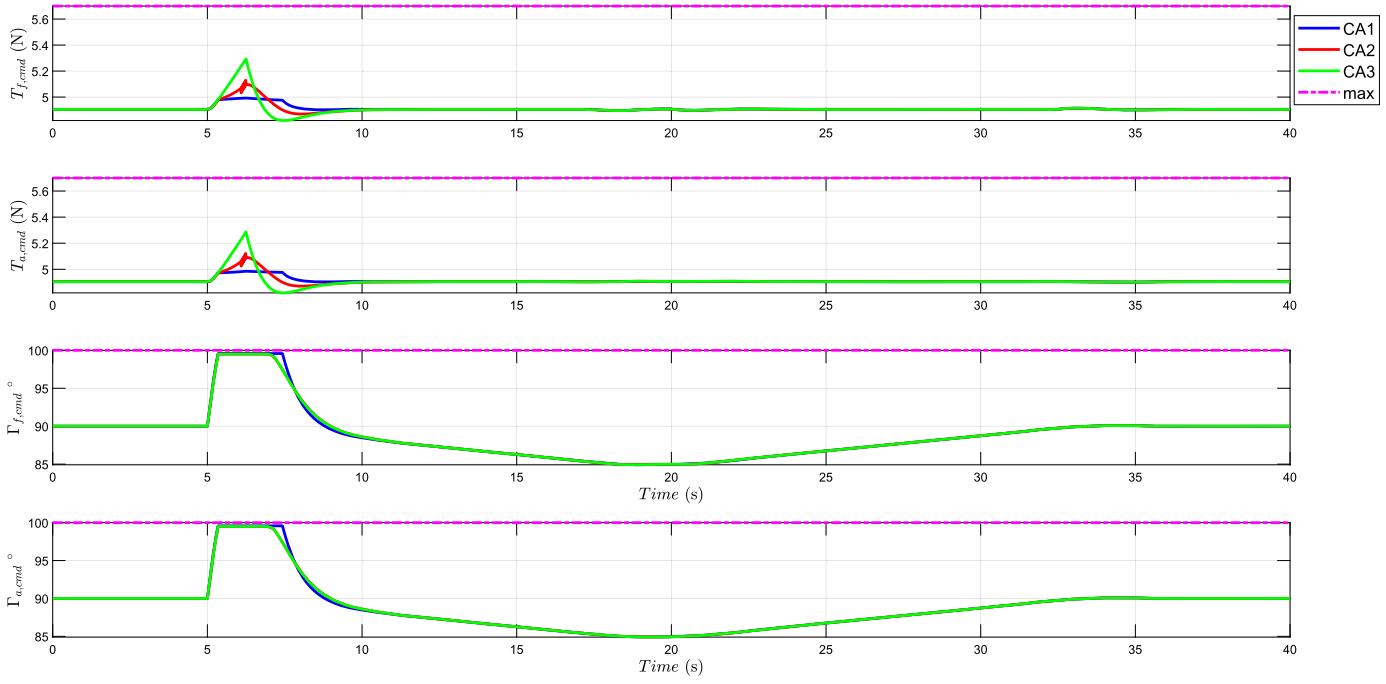

Fig. 19. Reverse backward and pitch control - Effector commands.

is active. Therefore, the CA algorithm finds the optimal solution quickly. Again, the CA algorithm does not cause discontinuities/sudden jumps in the actuator positions which is crucial for real time implementation.

6.3. Summary of control allocation approaches performance

Table 5 shows how the three CA approaches performed for the two manoeuvres in terms of tracking, constraints activated and number of CA iterations. No physical constraints were violated for all three CA approaches.

7. Conclusions

The results demonstrate that the control allocation can affectively allocate the overall control demand to the individual effectors and also impose effector constraints due to actuator saturation. The results also demonstrate the effectiveness of the proposed control allocation

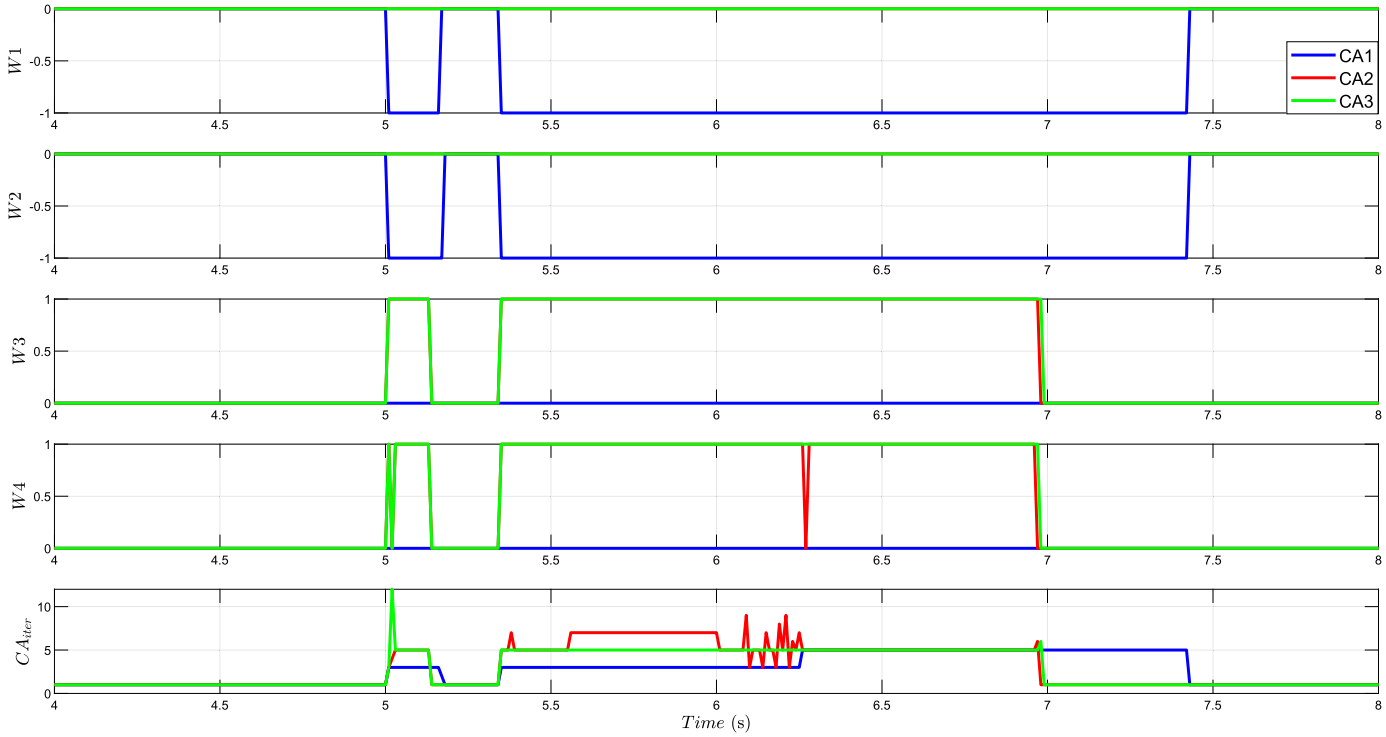

Fig. 20. Reverse backward and pitch control - Control limitation status.

Table 5
CA Approaches Performance Summary.

CA Approaches	Aircraft Manoeuvre	Tracking Performance	Constraints Activated	CA Iterations	Constraints Violated
CA 1	ACM 1	Excellent	$\overline{T}_{z,f}, \overline{T}_{z,r}$	5	None
CA 1	ACM 2	Excellent	$\underline{T}_{x,f}, \underline{T}_{x,r}$	5	None
CA 2	ACM 1	Excellent	$\overline{T}_f, \overline{T}_r, \overline{\Gamma}_f, \overline{\Gamma}_r, \dot{\overline{\Gamma}}_f, \dot{\overline{\Gamma}}_r$	7	None
CA 2	ACM 2	Excellent	$\overline{\Gamma}_f, \overline{\Gamma}_r$	7	None
CA 3	ACM 1	Good	$\overline{T}_f, \overline{T}_r, \overline{\Gamma}_f, \overline{\Gamma}_r, \dot{\overline{\Gamma}}_f, \dot{\overline{\Gamma}}_r$	11	None
CA 3	ACM 2	Good	$\overline{\Gamma}_f, \overline{\Gamma}_r$	11	None

schemes to allocate remaining control authority to higher priority and critical control channels in order to maintain operational safety and stability during certain flight conditions where there is limited control authority. All three control allocation schemes have similar performance but CA1 generally converges faster than CA2 and CA3. CA1 and CA3 will be more suitable for few actuators due to the complex nonlinear transformation of the effector constraints (position and rate) from polar to cartesian and the more complex LTV Effector mapping respectively. CA2 will be easier than CA1 and CA3 to implement for VTOL configurations with many redundant effectors due to its simplier LTV effector mapping (compared to CA3) and simpler transformation of effector limits from absolute to incremental. This active set algorithm can be solved in real-time (since it converges fast due to hot starting) on a modern flight control systems specifically for eVTOLs flight control computers which can have a processor speed over 1 GHz. Even with a worst case convergence of say 20 CA iterations (0.2 s) and for high bandwidth eVTOL electric actuators (up to 25 Hz designed to control the aeroelastic behaviour and flight mechanics of a model), it is tolerable.

To further develop the proposed CA Approach 2, state dependent effector models (e.g. traditional flight control surfaces like ailerons, rudders, flaps, slats, elevators etc. where the control effectiveness depends on airspeed) should also be tested. In order to test the full ability of the proposed CA Approaches 1, 2 and 3, a complete 6DoF eVTOL control scheme (including lateral-directional dynamics) and with representative aerodynamic model which has coupling between vectored thrust forces and dynamic forces should be designed and tested. Furthermore, since CA2 and CA3 are incremental, moment arm mismatch robustness test could be conducted to evaluate their robustness to effector model moment arm mismatch. Moreover, the adaptability of the CA schemes to actuator failures could be improved. Finally, Pilot-in-the-loop Full envelope testing of the 6DoF Model should be carried to assess the handing and flying qualities of aircraft.

CRediT authorship contribution statement

Emmanuel Enenakpogbe: Writing – original draft, Visualization, Validation, Supervision, Software, Resources, Project administration, Methodology, Investigation, Funding acquisition, Formal analysis, Data curation, Conceptualization. **James F. Whidborne:** Supervision. **Linghai Lu:** Supervision.

Funding

This research did not receive any specific grant from funding agencies in the public, commercial, or not-for-profit sectors.

Declaration of competing interest

The authors declare that they have no known competing financial interests or personal relationships that could have appeared to influence the work reported in this paper.

Data availability

No data was used for the research described in the article.

References

[1] M. Bodson, Evaluation of optimization methods for control allocation, J. Guid. Control Dyn. 25 (2002) 703–711, https://doi.org/10.2514/2.4937.

[2] Kenneth A. Bordignon, Constrained Control Allocation for Systems with Redundant Control Effectors, PhD thesis, Virginia Polytechnic Institute, VA, 1996, http://hdl.handle.net/10919/28570.

[3] Z.J. Chen, K.A. Stol, P.J. Richards, Preliminary design of multirotor UAVs with tilted-rotors for improved disturbance rejection capability, Aerosp. Sci. Technol. 92 (2019) 635–643, https://doi.org/10.1016/j.ast.2019.06.038.

[4] David Doman, Michael Oppenheimer, Improving control allocation accuracy for nonlinear aircraft dynamics, in: AIAA Guidance, Navigation, and Control Conference and Exhibit, 2002, p. 4667.

[5] Wayne Durham, Aircraft Flight Dynamics and Control, John Wiley & Sons, 2013.

[6] Wayne Durham, Kenneth A. Bordignon, Roger Beck, Aircraft Control Allocation, John Wiley, 2017.

[7] Emmanuel Enenakpogbe, James F. Whidborne, Linghai Lu, Control of an eVTOL using nonlinear dynamic inversion, in: 13th UKACC International Conference on Control (CONTROL 2022), 2022, pp. 158–164.

[8] Emmanuel Enenakpogbe, James F. Whidborne, Linghai Lu, Control of an over-actuated fixed-wing vectored thrust eVTOL, in: 14th UKACC International Conference on Control (CONTROL 2024), 2024, pp. 315–316.

[9] Isabelle Fantoni, Amparo Palomino, Nested saturation control for stabilizing the PVTOL aircraft, in: Unmanned Aerial Vehicles: Embedded Control, 2013, pp. 21–40.

[10] T.I. Fossen, T.A. Johansen, A survey of control allocation methods for ships and underwater vehicles, in: 14th Mediterranean Conference on Control and Automation, Ancona, Italy, 2006, pp. 1–6.

[11] Mohinder S. Grewal, Angus P. Andrews, Kalman Filtering: Theory and Practice with MATLAB, John Wiley & Sons, 2014.

[12] O. Härkegård, Quadratic programming control allocation toolbox (QCAT), MATLAB central file exchange, http://research.harkegard.se/qcat, 2004. (Accessed 8 October 2022).

[13] Ola Harkegard, Efficient active set algorithms for solving constrained least squares problems in aircraft control allocation, in: 41st IEEE Conference on Decision and Control (CDC2002), Las Vegas, NV, 2002, pp. 1295–1300.

[14] Ola Härkegård, Dynamic control allocation using constrained quadratic programming, J. Guid. Control Dyn. 27 (6) (2004) 1028–1034.

[15] Tor A. Johansen, Thor I. Fossen, Control allocation — a survey, Automatica 49 (5) (2013) 1087–1103, https://doi.org/10.1016/j.automatica.2013.01.035.

[16] Tor A. Johansen, Thomas P. Fuglseth, Petter Tøndel, Thor I. Fossen, Optimal constrained control allocation in marine surface vessels with rudders, Control Eng. Pract. 16 (4) (2008) 457–464, https://doi.org/10.1016/j.conengprac.2007.01.012.

[17] Namuk Kang, James Whidborne, Linghai Lu, Julien Enconniere, Scheduled flight control system of tilt-rotor VTOL PAV, in: AIAA SCITECH 2023 Forum, 2023, p. 1530.

[18] Lilium, Lilium GmbH. Lilium Jet, https://lilium.com. (Accessed 30 October 2022).

[19] I. Lindfors, Thrust allocation method for the dynamic positioning system, in: 10th International Ship Control Systems Symposium (SCSS 93), 1993, pp. 3–93.

[20] J. Littell, Challenges in vehicle safety and occupant protection for autonomous electric vertical take-off and landing (eVTOL) vehicles, in: AIAA Propulsion and Energy 2019 Forum, Number AIAA 2019-4504, Indianapolis, IN, 2019.

[21] Ya Liu, Fan Zhang, Panfeng Huang, Xiaozhen Zhang, Analysis, planning and control for cooperative transportation of tethered multi-rotor UAVs, Aerosp. Sci. Technol. 113 (2021) 106673, https://doi.org/10.1016/j.ast.2021.106673.

[22] Thomas Lombaerts, John Kaneshige, Stefan Schuet, Bimal L. Aponso, Kimberlee H. Shish, Gordon Hardy, Dynamic inversion based full envelope flight control for an eVTOL vehicle using a unified framework, in: AIAA Scitech 2020 Forum, 2020, p. 1619.

[23] Thomas Lombaerts, John Kaneshige, Stefan Schuet, Gordon Hardy, Bimal Aponso, Kimberlee H. Shish, Nonlinear dynamic inversion based attitude control for a hovering quad tiltrotor eVTOL vehicle, in: AIAA Scitech 2019 Forum, Number AIAA-2019-0134, San Diego, CA, 2019.

[24] Daniel Moses, Modelling and Simulation of an eVTOL with Distributed Propulsion Architecture, MSc thesis, Cranfield University, 2021.

[25] J. Nocedal, S.J. Wright, Numerical Optimization, Springer, 1999.

[26] SunHoo Park, Sihun Lee, Byeonguk Im, Dongyeol Lee, SangJoon Shin, Improvement of a multi-rotor UAV flight response simulation influenced by gust, Aerosp. Sci. Technol. 134 (2023) 108156, https://doi.org/10.1016/j.ast.2023.108156.

[27] J.A. Petersen, M. Bodson, Constrained quadratic programming techniques for control allocation, IEEE Trans. Control Syst. Technol. 14 (1) (2005) 91–98, https://doi.org/10.1109/TCST.2005.860516.

[28] J.A. Petersen, M. Bodson, Interior-point algorithms for control allocation, J. Guid. Control Dyn. 28 (3) (2005) 471–480, https://doi.org/10.2514/1.5937.

[29] K.O. Ploetner, C. Al Haddad, C. Antoniou, F. Frank, M. Fu, S. Kabel, C. Llorca, R. Moeckel, A.T. Moreno, A. Pukhova, et al., Long-term application potential of urban air mobility complementing public transport: an upper Bavaria example, CEAS Aeronaut. J. (2020) 1–17.

[30] Davi A. Santos, José A. Bezerra, On the control allocation of fully actuated multirotor aerial vehicles, Aerosp. Sci. Technol. 122 (2022) 107424, https://doi.org/10.1016/j.ast.2022.107424.

[31] O.J. Sørdalen, Optimal thrust allocation for marine vessels, Control Eng. Pract. 5 (9) (1997) 1223–1231.

[32] Jørgen Spjøtvold, Tor A. Johansen, Fault tolerant control allocation for a thruster-controlled floating platform using parametric programming, in: Proceedings of the 48h IEEE Conference on Decision and Control (CDC) held jointly with 2009 28th Chinese Control Conference, IEEE, 2009, pp. 3311–3317.

[33] Brian L. Stevens, Frank L. Lewis, Eric N. Johnson, Aircraft Control and Simulation: Dynamics, Controls Design, and Autonomous Systems, John Wiley, 2015.

[34] Anna Straubinger, Raoul Rothfeld, Michael Shamiyeh, Kai-Daniel Büchter, Jochen Kaiser, Kay Olaf Plötner, An overview of current research and developments in urban air mobility – setting the scene for UAM introduction, J. Air Transp. Manag. 87 (2020) 101852, https://doi.org/10.1016/j.jairtraman.2020.101852.

[35] E.C. Suiçmez, A.T. Kutay, Full envelope nonlinear flight controller design for a novel electric VTOL (eVTOL) air taxi, Aeronaut. J. 128 (1323) (2023) 966–993, https://doi.org/10.1017/aer.2023.87.

[36] Emre Can Suiçmez, Full Envelope Nonlinear Controller Design for a Novel Electric VTOL (eVTOL) Air-taxi via INDI Approach Combined with CA, PhD thesis, Middle East Technical University, 2021, https://hdl.handle.net/11511/90898.

[37] Calvin Ming Hao Tan, Multidisciplinary modeling & simulation framework for electric vertical take-off &, landing (eVTOL) vehicles, 2020.

[38] Vertical Flight Society, Vertical Flight Society announces continued strong growth, https://vtol.org/files/dmfile/vfspressrelease-2020growth_200113.pdf. (Accessed 30 October 2020).

[39] Yongchao Wang, Yaoming Zhou, Chenghao Lin, Modeling and control for the mode transition of a novel tilt-wing UAV, Aerosp. Sci. Technol. 91 (2019) 593–606, https://doi.org/10.1016/j.ast.2019.05.046.

[40] James F. Whidborne, Alastair K. Cooke, Gust rejection properties of VTOL multirotor aircraft, IFAC-PapersOnLine 50 (2) (2017) 175–180, https://doi.org/10.1016/j.ifacol.2017.12.032.

[41] James F. Whidborne, Arthur P. Mendez, Alastair Cooke, Effect of rotor tilt on the gust rejection properties of multirotor aircraft, Drones 6 (10) (2022) 305, https://doi.org/10.3390/drones6100305.

[42] Kewei Xia, Sangheon Lee, Hungsun Son, Adaptive control for multi-rotor UAVs autonomous ship landing with mission planning, Aerosp. Sci. Technol. 96 (2020) 105549, https://doi.org/10.1016/j.ast.2019.105549.

[43] Yunjie Yang, Jihong Zhu, Xiaming Yuan, Xiangyang Wang, Minchi Kuang, Heng Shi, Dynamic characteristics analysis and robust transition control of tail-sitter VTOL UAVs, Aerosp. Sci. Technol. 145 (2024) 108868, https://doi.org/10.1016/j.ast.2024.108868.

[44] G.J.J. Ducard, M. Allenspach, Review of designs and flight control techniques of hybrid and convertible VTOL UAVs, Aerosp. Sci. Technol. 118 (2021) 1–25, https://doi.org/10.1016/j.ast.2021.107035.

[45] Ola Härkegård, Backstepping and Control Allocation with Application to Flight Control, PhD thesis, Linkoping University, Linkoping, Sweden, 2003.

https://dspace.org/

Control allocation problem transformation approaches for over-actuated vectored thrust VTOLs

Enenakpogbe, Emmanuel; Whidborne, James F.; Lu, Linghai

2025-06-01
Elsevier
https://doi.org/10.1016/j.ast.2025.110145
Enenakpogbe E, Whidborne JF, Lu L. (2025) Control allocation problem transformation approaches for over-actuated vectored thrust VTOLs. Aerospace Science and Technology, Volume 161, June 2025, Article number 110145

Downloaded from a DSpace repository. https://dspace.org/